Check for updates

The Meteoritical Society

Meteoritics & Planetary Science 58, Nr 10, 1449–1468 (2023)
doi: 10.1111/maps.14060

Linking meteorites to their asteroid parent bodies: The capabilities of dust analyzer instruments during asteroid flybys

Lisa Maria ECKART[1,2], Jon K. HILLIER[1]*, Frank POSTBERG[1], Simone MARCHI[3], and Zoltan STERNOVSKY[4]

[1]Freie Universität Berlin, Berlin, Germany
[2]ETH Zürich, Zürich, Switzerland
[3]Southwest Research Institute, Boulder, Colorado, USA
[4]University of Colorado Boulder, Boulder, Colorado, USA
***Correspondence**
Jon K. Hillier, Freie Universität Berlin, Berlin, Germany.
Email: j.hillier@fu-berlin.de

(Received 16 December 2022; revision accepted 15 July 2023)

Abstract–Linking meteorites to their asteroid parent bodies remains an outstanding issue. Space-based dust characterization using impact ionization mass spectrometry is a proven technique for the compositional analysis of individual cosmic dust grains. Here we investigate the feasibility of determining asteroid compositions via cation mass spectrometric analyses of their dust ejecta clouds during low (7–9 km s^{-1}) velocity spacecraft flybys. At these speeds, the dust grain mass spectra are dominated by easily ionized elements and molecular species. Using known bulk mineral volume abundances, we show that it is feasible to discriminate the common meteorite classes of carbonaceous chondrites, ordinary chondrites, and howardite–eucrite–diogenite achondrites, as well as their subtypes, relying solely on the detection of elements with ionization efficiencies of ≤700 or ≤800 kJ mol^{-1}, applicable to low (~7 km s^{-1}) and intermediate (~9 km s^{-1}) flyby speed scenarios, respectively. Including the detection of water ion groups enables greater discrimination between certain meteorite types, and flyby speeds ≥10 km s^{-1} enhance the diagnostic capabilities of this technique still further. Although additional terrestrial calibration is required, this technique may allow more unequivocal asteroid-meteorite connections to be determined by spacecraft flybys, emphasizing the utility of dust instruments on future asteroid missions.

INTRODUCTION

Asteroids are remnants of planet accretion and the understanding of their composition and diversity provides important constrains on the conditions and processes that occurred in the early Solar System. The primary method for studying the composition of asteroids is via remote sensing observations—for example, reflectance spectroscopy and photometry (e.g., Bus et al., 2002; DeMeo et al., 2015; Emery et al., 2019; Gaffey et al., 1993; Li et al., 2015; Reddy et al., 2015). These works have provided the basis for asteroid taxonomical classifications with a wealth of data for thousands of asteroids. Despite these successes, the compositional make-up of most asteroids remains elusive. Furthermore, other factors, such as atmospheric transmission, observation geometry (e.g., phase angle) and physical properties (e.g., surface grain size distribution and temperature) often complicate the interpretation of remote sensing data (e.g., Gaffey, 2010; Hinrichs et al., 1999; Le Bras & Erard, 2003). In addition, many asteroids show rather featureless reflectance spectra (e.g., Carvano et al., 2003; Cloutis et al., 1990; Licandro et al., 2008), making the compositional analysis challenging.

Since the pioneering work of Wylie (1939), asteroids have been recognized as the major source of meteorites. Asteroid samples thus can be studied in the laboratory using sophisticated tools for analysis. However, linking

© 2023 The Authors. *Meteoritics & Planetary Science* published by Wiley Periodicals LLC on behalf of The Meteoritical Society.
This is an open access article under the terms of the Creative Commons Attribution License, which permits use, distribution and reproduction in any medium, provided the original work is properly cited.

meteorites to their asteroid parent bodies remains an outstanding issue, with many open questions and gaps remaining. Typically, meteorites and asteroids are linked through reflectance spectra (e.g., Gaffey et al., 1993; Miyamoto et al., 2018; Pieters & McFadden, 1994), requiring laboratory measurements of meteorite reflectance spectra, as well as those of asteroids. However, asteroid surface alteration due to "space weathering" (including processes caused by exposure to cosmic rays, solar wind, and micrometeorite bombardment; for example, Chapman et al., 1996, 2004; Gaffey, 2010) and meteorite alteration by terrestrial weathering, together with the dependence of reflectance spectra on physical properties of the meteorite sample and asteroid surface (e.g., grain size and temperature; Hiroi & Pieters, 1992; Moroz et al., 2000) complicate the comparisons between asteroid and meteorite spectra. In a comprehensive study, DeMeo et al. (2022) compared 500 asteroid spectra with over 1000 meteorite spectra in the visible and near-infrared wavelength regions (0.45–2.5 μm). Although well-established asteroid-meteorite connections were confirmed, and new possible links were proposed, many relations remain uncertain due to the non-unique and often featureless spectral characteristics of many asteroids (e.g., C-, B-, D- and X-type asteroids). For example, X-type asteroids show weak spectral absorption features in the visible and near-infrared wavelengths and can be associated with carbonaceous chondrites (CCs), enstatite chondrites, aubrites, or iron meteorites (DeMeo et al., 2022). In order to resolve the ambiguity, there is a need for complementary measurement methods to determine the specific meteorite links (DeMeo et al., 2022). In particular, it is interesting to note that these asteroid-meteorite associations are generally valid for broad taxonomic complexes (e.g., ordinary chondrites, OC are predominantly associated with S-complex asteroids), rather than individual asteroids. Also, many asteroids appear not to be represented in our meteorite collections (DeMeo et al., 2022). In spite of this progress, only one definitive meteorite-asteroid link has been established so far: the howardite–eucrite–diogenite (HED) meteorites with asteroid Vesta (e.g., Binzel & Xu, 1993; Miyamoto & Takeda, 1994). It is estimated that known meteorites may sample some 100–150 parent bodies (Greenwood et al., 2020), and most of those are distinct iron meteorites from shattered parent bodies. This implies that many large, primordial asteroids (>100 km) appear not to be represented in the current meteorite collection (Greenwood et al., 2020).

In view of the challenges of linking asteroids and meteorites, an alternative technique has recently been proposed by Cohen et al. (2019). They suggest identifying the meteorite analog of an asteroid (if represented in the terrestrial collection) by analyzing dust particles ejected from the surface, which are detected during spacecraft flyby using impact ionization mass spectrometry. However, since the resulting mass spectra are a function of the impact speed of the incoming dust particle (and hence flyby speed of the spacecraft), the technique described by Cohen et al. (2019) is only applicable to higher flyby speed missions (>15 km s^{-1}). In the following, we briefly summarize the original Cohen et al. technique and the principles of spacecraft flyby dust detection. Subsequently, we present new approaches which are valid for flyby speeds as low as 7–9 km s^{-1}.

In Situ Compositional Analysis of Asteroids During Spacecraft Flyby

Airless bodies, including asteroids (Szalay & Horányi, 2016), the Moon (Horányi et al., 2015), and the moons of Jupiter (Krüger et al., 1999, 2000) are surrounded by dust ejecta clouds produced by the continual bombardment and excavation of surface materials by high-velocity impacts of interplanetary micrometeoroids. By passing through this dust cloud a spacecraft carrying a dust mass spectrometer can measure the compositions of the ejected surface grains individually and with a suitably large dust sample size, determine the broad composition of surface materials, as well as determine the possible relationship to meteorite types (Cohen et al., 2019).

Cohen et al. (2019) separated the mineralogical components of meteorites into broad compositional classes that are expected to be distinguishable using impact ionization mass spectrometry (silicates, Fe-Ni metal, phosphates and sulfides, and oxides), with the Fe/Mg ratio of silicates used as a further discriminator. Using Monte Carlo simulations, in which distributions of monomineralic grain compositions were generated based on the bulk abundance of the respective meteorite phases, Cohen et al. (2019) showed that as few as 20 particles detected (and their mass spectra measured) are sufficient to distinguish between major meteoritic classes, and meteorite group discrimination was possible with 200–700 grains. The method was then tested on the sample of 1087 monomineralic dust grains returned by the *Hayabusa* spacecraft (Nakamura et al., 2011), compositionally identifying asteroid (25143) *Itokawa* as an LL-chondrite via the analysis of as few as 200 grains. The authors then proceed to show that Near-Earth Asteroids (NEOs, 1–1.5 AU heliocentric distance) larger than 10 km would provide a statistically sufficient number (>100) of ejecta particles for flyby distances below 100 km. These estimates are for a 600 cm^2 effective collection area of the dust detector and particles larger than 50 nm in radius, and are based on extending the findings of the recent LADEE measurements of Moon's

19455100, 2023, 10, Downloaded from https://onlinelibrary.wiley.com/doi/10.1111/maps.14060 by Freie Universitaet Berlin, Wiley Online Library on [16/10/2023]. See the Terms and Conditions (https://onlinelibrary.wiley.com/terms-and-conditions) on Wiley Online Library for rules of use; OA articles are governed by the applicable Creative Commons License

ejecta clouds (Pokorný et al., 2019). Generally, larger asteroids have denser ejecta clouds, and more particles can be detected and analyzed at closer flyby distances.

However, the approach outlined by Cohen et al. uses mass spectral metrics which are likely to be only fully applicable at dust impact velocities (and hence flyby speeds) greater than about 15 km s^{-1}. Flyby speeds of near-Earth asteroids and main belt asteroids vary considerably, depending on spacecraft trajectory and destination (Farquhar et al., 2002). The findings of Cohen et al. (2019) are applicable for the planned flyby of asteroid (3200) Phaethon by DESTINY Plus (~30 km s^{-1}), or that of (9969) Braille at 15.7 km s^{-1} by Deep Space 1. However, other flybys, such as Stardust's 7.4 km s^{-1} flyby of (5535) Annefrank or Rosetta's 8.6 km s^{-1} flyby of (2867) Steins, occurred at much lower speeds, too low for the reliable detection or quantification of some of the common constituents of minerals.

Impact Ionization Mass Spectrometry

Measuring the composition of dust ejecta particles from an asteroid during a flyby requires an impact ionization mass spectrometer that is capable of analyzing micron and sub-micron sized particles. The capabilities of dust analyzers were demonstrated, for example by Cassini's Cosmic Dust Analyzer (CDA, Srama et al., 2004). There are several dust analyzer instruments currently in development with capabilities much exceeding those of CDA, including the Surface Dust Analyzer (SUDA) for the Europa Clipper mission (Kempf et al., 2014), the DDA instrument for the DESTINY Plus mission (Srama et al., 2019), or the Interstellar Dust Experiment (IDEX) instrument for the Interstellar Mapping and Acceleration Probe (IMAP, McComas et al., 2018). In case of the SUDA, the instrument will be capable of mapping the compositional variations of Europa's surface and correlating the composition of individual ejecta particles to surface features (Goode et al., 2021; Postberg et al., 2011).

The measurement principle for this technique of time-of-flight mass spectrometry (ToF-MS) is based on impact ionization, where particles impacting onto a metal target at speeds above about 2 km s^{-1} generate an impact plasma (e.g., Friichtenicht & Slattery, 1963). The composition of the impact plasma cloud depends upon that of the projectile (i.e., the impacting dust grain) and the target material and varies strongly with impact speed (e.g., Drapatz & Michel, 1974) and, to a lesser extent, particle mass. Generally, with increasing impact speed or particle mass (and therefore available kinetic energy), elements with higher ionization energies appear in the plasma, and the fraction of molecular ions decreases (see, e.g., Fiege et al., 2014; Hillier et al., 2014). The ions from the impact plasma are extracted and analyzed using ToF-MS. Although large grains will produce more ions and higher amplitude spectral signals, the role that mass plays in the velocity threshold (the relative impact speeds at which particular ions appear regularly in the mass spectra) has not yet been investigated. In part, this is because the terrestrial calibration of impact ionization mass spectrometers uses electrostatic accelerators, which accelerate grains to the same kinetic energy, producing a link between grain size (mass) and achieved velocity. Experiments to accelerate using lower accelerator potentials are planned in the near future, to investigate the behavior of "small and slow" impactors, but the other population—large and fast, is out of reach of existing equipment. We also note that the technique of Cohen et al. (2019), as well as that presented here (described in detail in the Methods section), relies upon the assumption of monomineralic grains, most likely to occur at radii smaller than 100 nm (Cohen et al., 2019). Larger particles, with an accompanying increase in available kinetic energy for a given impact speed, although potentially subject to different "velocity" thresholds, are therefore less likely to be monomineralic and instead produce spectra that are too complex to be included in this analysis (see Discussion section).

The likelihood of a given element appearing in a mass spectrum of ions extracted from the plasma is determined by (1) its abundance in the grain, (2) ionization energy of the element, (3) the available energy (kinetic energy of the impact and energy partitioning between the target/projectile materials), and (4) matrix and plasma effects in the impact cloud (e.g., Fiege et al., 2014; Hillier et al., 2012). The combination of these effects is illustrated by the elemental/molecular ion velocity thresholds and relative sensitivity factors (RSFs, enabling quantitative derivation of particle composition). The velocity thresholds derived for elements within orthopyroxene (Fiege et al., 2014) clearly indicate that low-speed (7–9 km s^{-1}) flybys would not produce reliable and abundantly ions of the elements required for the techniques proposed by Cohen et al. (2019). These use the abundances of silicates, Fe-Ni metal, sulfides, phosphates, and oxides; however, the primary constituents of those phases are not reliably detected below 10 km s^{-1}. Derivation of RSFs, which allow the original grain mineral composition to be quantitatively derived from elemental spectral abundances, has so far only been demonstrated for impacts at speeds ≥19 km s^{-1} (Fiege et al., 2014). However, ions of easily ionized elements, such as, for example, Na, K, Ca, Al, and Mg, do appear at measurable levels at much lower speeds. Existing data for rock-forming cations (e.g., Fiege et al., 2014; Hillier et al., 2012, 2018; Mocker et al., 2013), indicates elements with ionization energy of ≤700 kJ mol^{-1}, along with Mg,

19455100, 2023, 10, Downloaded from https://onlinelibrary.wiley.com/doi/10.1111/maps.14060 by Freie Universitaet Berlin, Wiley Online Library on [16/10/2023]. See the Terms and Conditions (https://onlinelibrary.wiley.com/terms-and-conditions) on Wiley Online Library for rules of use; OA articles are governed by the applicable Creative Commons License

should appear in spectra at speeds of ≥7 km s^{-1}, and those with ionization energies ≤800 kJ mol^{-1} should appear at impact speeds ≥9 km s^{-1}.

In this study, we demonstrate that distinguishing between various meteorite classes and groups remains possible, if solely elements are considered that are assumed to be reliably detected at low- to intermediate flyby speeds. As with Cohen et al. (2019), we focus on elements that are measured using a cation spectrometer. We differentiate between the two cases of 7 km s^{-1} (low) and 9 km s^{-1} (intermediate) flyby speed, resulting in spectra produced by elements with maximum ionization energies of 700 and 800 kJ mol^{-1}, respectively. Additionally, we assume water group ions, such as OH^+, H_2O^+, and H_3O^+, to be identifiable among spectra in both speed cases, building upon results from laboratory dust acceleration experiments by Hillier et al. (2018). All methods presented in the following are also applicable at higher flyby speeds, until the available impact energies begin to dissociate any molecular species (for example, the previously mentioned water group ions; Hillier et al., 2018). The present study expands upon the work of Cohen et al. (2019) and investigates the value of dust impact analyzer instruments in the classification of meteorites and asteroids at these lower speeds.

METHODS

An initial set of meteorite types was chosen based upon their currently postulated matches to some of the most common asteroid classes in the main belt, and the availability of suitably detailed mineralogical/petrological information about the meteoritic composition. The resulting asteroid/meteorite pairings are described briefly in the following. C-type asteroid spectroscopic features match best with laboratory spectra of CCs (Feierberg et al., 1981). This is a class of undifferentiated, primitive meteorites that consists mainly of (partially hydrated) silicate minerals containing up to 5 wt% carbon (in the form of organic compounds, carbonates, and presolar grain material such as graphite, diamond, and silicon carbide; Gilmour, 2003), as well as refractory material in the form of calcium-aluminum-rich inclusions (CAIs). CCs have a variety of subtypes, for example, CI, CM, CV, and CR, with each group possibly sampling a distinct asteroid parent body.

Reflectance spectra of S-type asteroids indicate a siliceous (i.e., stony) mineralogic composition composed mostly of olivine and low-calcium pyroxene. Their link to OCs, the most abundant meteorite type (>85% in the meteorite collection) has been generally accepted, after samples from the S-type asteroid (25143) *Itokawa* were returned to Earth by the *Hayabusa* mission and subsequently classified as thermally metamorphosed LL chondrite (Nakamura et al., 2011). The three subtypes of OCs, H, L, and LL, refer to the varying amounts of iron and metal (H for high total iron and high metal, L for lower total iron and metal, and LL for low total and metallic iron).

The relationship between Vesta and its family members (Vestoids) with the HED meteorites is currently the best-established asteroid-meteorite connection (McCord et al., 1970; McSween & Binzel, 2022). While eucrites and diogenites are thought to represent parts of Vesta's crust and mantle, respectively, and therefore closely resemble terrestrial igneous rocks, howardites are polymict breccias containing pieces of both, sometimes containing intermixed chondritic material and impact melt.

For the above meteorite groups, we collected published data of the modal mineral volume abundances of 136 samples (see Table A1). Where mineral abundances were given in wt%, we used typically applicable mineral densities to convert them into vol%. The data and corresponding references can be found in Table A1. We note that the published analyses of meteorite compositions are themselves typically undertaken at lower spatial resolutions than the grain sizes assumed in this work, and this may introduce minor, unquantifiable, errors to the quoted mineral abundances. We considered 1 vol% as a lower limit mineral abundance to account for variations in the measured meteorite compositions, as well as to provide the statistical best-case likelihood of detecting at least one grain from a given component among 100 spectra. In reality, a larger sample of grains is likely to be required, as —depending on the scale—the micrometeorite impact ejection process may, as well as stochastically sampling the surface of the asteroid, produce multiple grains with identical compositions, or different yields from different materials. At the exact time of any flyby, the steady state dust cloud composition may therefore deviate from the ideal perfectly sampled composition. As with Cohen et al. (2019), we assume a simple case where the asteroid's surface is composed of a single meteorite type and shed dust grains are monomineralic, resulting in dust clouds dominated by particles whose compositional abundances mirror those of the parent asteroid (and hence possibly connected meteorite type). The latter assumption is based on the Itokawa grain size/composition distribution determined by Nakamura et al. (2011) and extrapolation of grain composition with size from the Stardust collection (Brownlee et al., 2006; Hörz et al., 2006), where grains with radii <100 nm were mostly monomineralic in nature. In this work, we do not consider the possibility that the yield of impacts into different materials may be different—that is, an impact onto a metal may produce far fewer ejecta grains than one onto a rocky surface, introducing a bias to the ejecta cloud population. We also assume that

19455100, 2023, 10, Downloaded from https://onlinelibrary.wiley.com/doi/10.1111/maps.14060 by Freie Universitaet Berlin, Wiley Online Library on [16/10/2023]. See the Terms and Conditions (https://onlinelibrary.wiley.com/terms-and-conditions) on Wiley Online Library for rules of use; OA articles are governed by the applicable Creative Commons License

space weathering processes—such as the formation of nanoscale Fe (e.g., Pieters et al., 2000)—do not affect the mass spectral appearance of the grains, or in the cases where it may, the contributions from these species are negligible in comparison with those from the bulk minerals.

Several approaches were developed upon which the three meteorite classes (CCs, OCs, and HEDs), as well as their groups, may be discriminated based on the easily ionized components of their mineralogy, as detected by a dust impact ionization mass spectrometer during spacecraft flyby. As previously mentioned, we consider two distinct cases:

1. A low-speed flyby case at ~7 km s^{-1}, including all elements with an ionization efficiency of ≤700 kJ mol^{-1} (such as, e.g., K, Na, Al, Ca) plus additionally Mg, as its cations are known to be produced and easily recognizable at very low impact speeds (Fiege et al., 2014; Hillier et al., 2018).
2. An intermediate-speed flyby case at ~9 km s^{-1}, encompassing all elements with ionization efficiencies of ≤800 kJ mol^{-1} (thus including, e.g., Fe, Ni, Si, S, and P).

Moreover, we assume in both cases to be able to identify the presence of water ions (from OH and H_2O) based on laboratory-derived spectra from Hillier et al. (2018), although further research is underway to demonstrate both hydroxylated and hydrated minerals can be reliably identified and distinguished using a cation spectrometer. While each spectrum represents a single monomineralic dust grain intercepting the dust detector and may identify a specific mineral simply upon the appearance of typical elements, the frequency of a spectra type—that is, the same elemental assemblage—may consequently reveal the abundance of a mineral phase (or category) among the dust cloud flown through. Elemental ratios can be derived within an ensemble of a spectral type to derive the average composition of the mineral, or equally for the sum of the spectra, representing the bulk elemental dust cloud composition.

Although earlier spectrometers, such as CDA, had targets that contained some slight contamination (e.g., Na, K) at launch (Postberg et al., 2009), this issue is now understood, and greater care is taken to produce and maintain contaminant-free impact targets. Ground calibration of such instruments is also often plagued by anthropogenic alkali earth metal contamination (Postberg et al., 2009), or from contamination introduced during the production of accelerable dust analogs (e.g., Hillier et al., 2018 used salts that contained both Na and K). Revised laboratory methodology and new coating techniques are currently being developed to prevent the introduction of mineral/sample-relevant compounds.

RESULTS

Distinguishing Between Meteorite Classes

In both the low and intermediate-speed cases, we find that distinguishing between the meteorite classes of CCs, OCs, and HED achondrites is possible. At 7 km s^{-1}, the three classes are best discriminated using the number of spectra (grain detections) of plagioclase, which are recognized by the simultaneous presence of Ca, Na and Al without Mg, in combination with the average plagioclase composition (obtained from the sum of their spectra; Figure 1). As plagioclase comprises a major phase in howardites and eucrites (on average 36 and 45 vol%, respectively, cf. Table A1) and is calcium-rich (with $An_{80\text{-}95}$; e.g., Rubin, 1997), an ensemble of spectra gathered during a flyby of a Vestoid should be distinguishable from those of an S-type asteroid analogous to OCs, with the latter exhibiting intermediate modal abundances of sodic plagioclase (on average 12 vol% with typically $An_{9\text{-}14}$; Brearley & Jones, 1998; Nakamuta & Motomura, 1999; although there were also more calcic feldspar grains found among chondrules of L/LL4 Bjurböle with An_{43} on average; Kovach & Jones, 2010) and a C-type asteroid analogous to CCs (considering only CI, CM, CV, CR) that contain rare to no plagioclase (anorthite is present above the detection limit of 1 vol% only in CV chondrites; Howard et al., 2010; and typically ranges between $An_{80\text{-}100}$; Brearley & Jones, 1998). Similar to CVs, diogenites contain only small amounts of plagioclase (~2 vol% on average), and their composition is very calcic ($An_{85\text{-}90}$; e.g., Rubin, 1997). Detecting a spectrum, which simultaneously contains Ca and Ti without Mg—likely to derive from, for example, perovskite or hibonite—would further indicate a CC-like composition of the asteroid's surface, as both phases can appear in refractory CAIs, which OCs and HEDs completely lack.

At 9 km s^{-1} and above, elements such as Fe, Si, O, S, and P begin to appear in the mass spectra, making the identification of various mineral types, such as further silicates, sulfides, and metals, possible. In this speed regime, distinguishing between CCs, OCs, and HED achondrites—in addition to the low-speed method—was found to be possible by comparing the amount of detected olivine with that of low-Ca pyroxene (LCP; both discriminable using the (Mg + Fe)/Si ratio in the spectrum, which is 1 in the case of LCP and 2 for olivine; see Figure 2). In some cases, the olivine/LCP ratio will not be sufficient to discriminate the three meteorite classes and require additional parameters to be used. This could be, for instance, the presence of phyllosilicates, recognized by a water ion peak, to further aid in discriminating CRs from OCs. To separate very olivine-

19455100, 2023, 10, Downloaded from https://onlinelibrary.wiley.com/doi/10.1111/maps.14060 by Freie Universitaet Berlin, Wiley Online Library on [16/10/2023]. See the Terms and Conditions (https://onlinelibrary.wiley.com/terms-and-conditions) on Wiley Online Library for rules of use; OA articles are governed by the applicable Creative Commons License

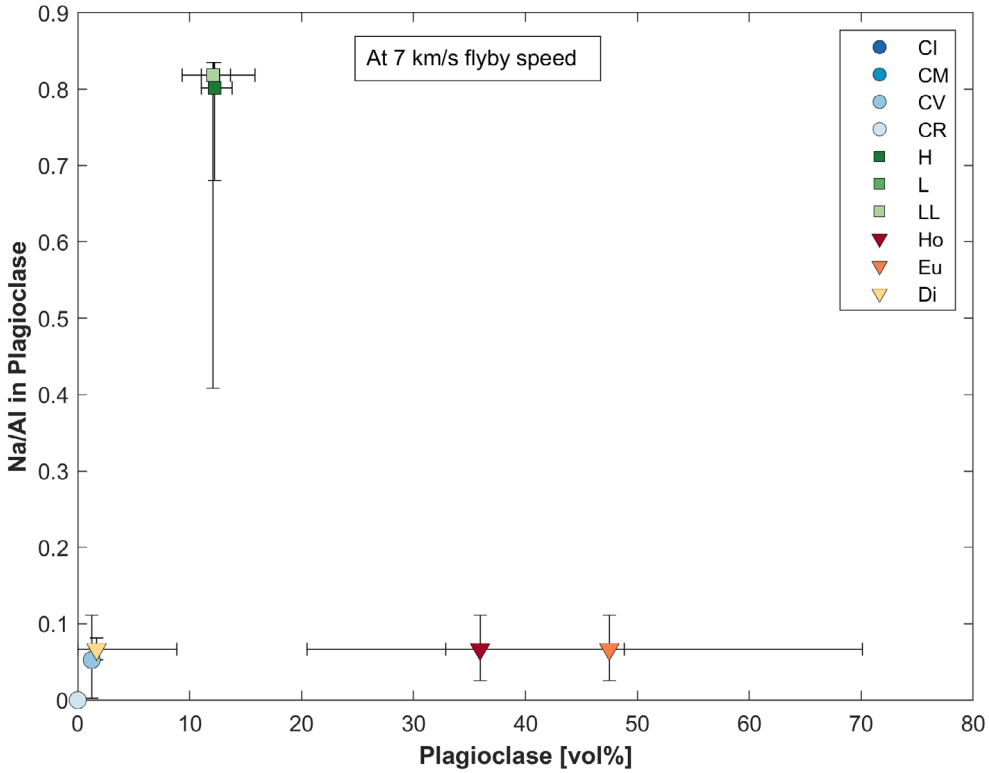

FIGURE 1. Discriminating between carbonaceous chondrites, ordinary chondrites and howardite–eucrite–diogenite achondrites at 7 km s^{-1} flyby speed by means of plagioclase abundance and its average composition (see text for details and references) in the bulk meteorite. Plagioclase is recognized by the simultaneous appearance of Ca, Na and Al without Mg among an individual spectrum. (Color figure can be viewed at wileyonlinelibrary.com)

rich diogenites, such as NWA 2968 and MIL 03443, from CV chondrites, it may be possible to use spectra with strong Ca and Al peaks deriving from the impact of a CAI phase, which is abundant among CVs, but lacking in ultramafic diogenites.

Discriminating Between Meteorite Groups

At flybys of 7 km s^{-1} and above, we find that also identifying the meteorite groups of OCs, CCs, and HED is to some extent feasible. The three groups of HED achondrites, howardites, eucrites, and diogenites may again be distinguished using the bulk plagioclase content as was already applied for the discrimination of meteorite classes (see Figure 1). However, since the plagioclase abundances of both howardites and eucrites overlap within their bulk compositional variations, their unequivocal classification may not be entirely possible, although a higher abundance of plagioclase spectra would still favor a eucritic composition. Additionally, it is possible that howardites contain some phyllosilicates because they are regolith breccias of eucrites and diogenites, and are occasionally intermixed with chondritic material. Thus they may produce some water-rich spectra that are unlikely to be detected from a eucritic (basaltic) rock composition.

In the case of CCs, we find that distinguishing between CI, CM, CV, and CRs is challenging but possible. CI, CM, and CRs have typically experienced moderate to strong aqueous alteration as part of their parent bodies, leading to the (partial) replacement of anhydrous silicates by phyllosilicates. Hence, their spectra will show peaks from water ions, in contrast to those of CVs, which are usually dry and do not contain notable amounts of water (although some oxidized subtypes exist with small amounts of phyllosilicates between 1.9 and 4.2 vol%; Howard et al., 2010). Moreover, the matrix of CIs generally contains higher amounts of saponite, which is only a minor phase in CMs, being dominated by serpentine minerals (e.g., Zolensky et al., 1993). A high number of spectra containing hydrated peaks together with Na, Al, and Mg would therefore favor a CI-like composition.

Also, the CAI abundance and mineralogy may be important for separating the CC groups. CAIs are most frequent in CVs (with abundances varying among different studies between 0.65 area% to 9.4 vol%; May et al., 1999; McSween, 1977) and contain abundant

19455100, 2023, 10, Downloaded from https://onlinelibrary.wiley.com/doi/10.1111/maps.14060 by Freie Universitaet Berlin, Wiley Online Library on [16/10/2023]. See the Terms and Conditions (https://onlinelibrary.wiley.com/terms-and-conditions) on Wiley Online Library for rules of use; OA articles are governed by the applicable Creative Commons License

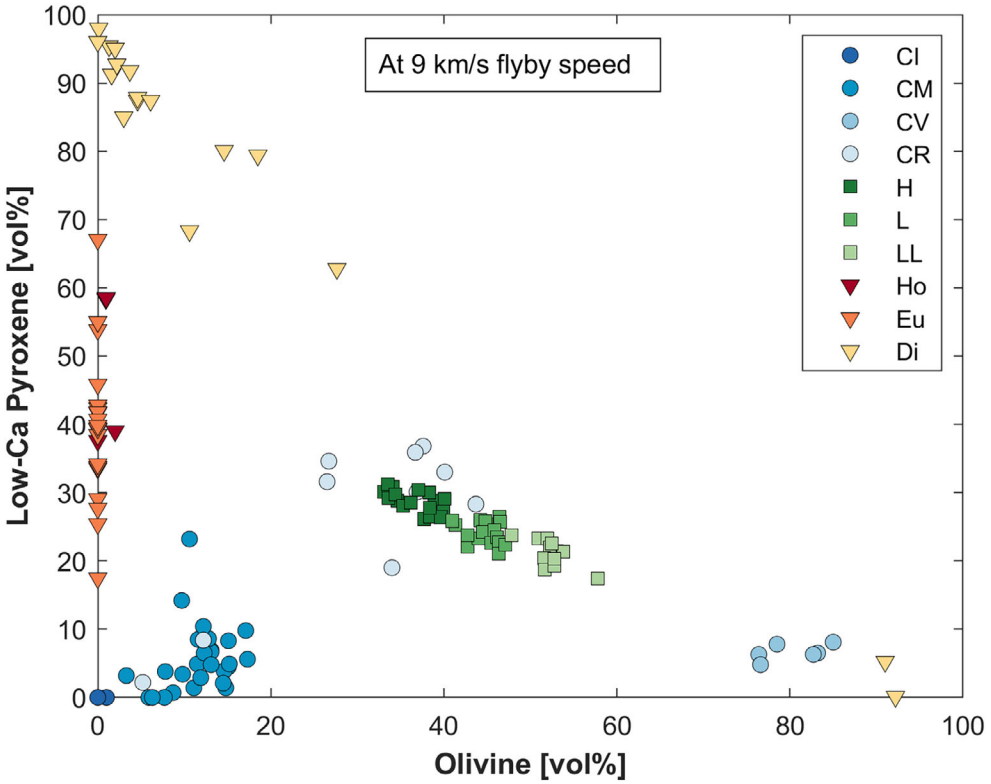

FIGURE 2. Discriminating between carbonaceous chondrites, ordinary chondrites and howardite–eucrite–diogenite achondrites at 9 km s^{-1} flyby speed by means of olivine versus low-Ca pyroxene abundance. Olivine and low-Ca pyroxene are distinguished upon their (Mg + Fe)/Si ratio among the individual spectra. (Color figure can be viewed at wileyonlinelibrary.com)

melilite and anorthite. These are phases that CAIs of CMs are typically devoid of (e.g., MacPherson, 2014) while containing abundant Ti-rich hibonite, a phase rarely occurring in CVs (CAI abundance in CMs ranges between ~0.5–3.8 vol%; Hezel et al., 2008; Norton & McSween, 2007; Rubin, 2015). CAIs among CI and CR chondrites are expected to be below the detection limit of 1 vol% for 100 dust samples. Consequently, detecting spectra from CAI phases, together with those of hydrated minerals, would point towards a CM-like composition, while detecting only CAI spectra without evidence of water would favor a CV-like composition. As both, CI and most CR chondrites are strongly to moderately aqueously altered, their separation might not be entirely possible at encounter speeds of ≤7 km s^{-1}, although a high number of spectra with hydrated features would favor a classification as CI-like.

Alternatively, Kallemeyn and Wasson (1981) found that the CC groups of CI, CM, CV, and also CO chondrites can be separated using their bulk Ca/Mn vs. Al/Mn ratios (Figure 3). The ionization energy of Mn is slightly above 700 kJ mol^{-1}, but still below that of Mg. It would therefore be interesting to investigate the velocity threshold of Mn in future laboratory calibration campaigns. If it proves to be ≤7 km s^{-1}, the method proposed by Kallemeyn and Wasson (1981) could also be applied to discriminate between the four CC groups. The bulk atomic ratios are thereby derived from the sum of the obtained spectra.

In the case of H, L, and LL OCs, discriminating between the three groups is found to be challenging at a 7 km s^{-1} flyby, as the energy of an impact would not suffice to ionize Fe, the key element for distinguishing the three subtypes. However, in that case, we propose to draw conclusions from the various spectra categories produced. Since OCs are essentially composed of olivine and LCP (two-thirds to three-fours), as well as HCP, plagioclase, FeNi-metal, and sulfide, four different types of spectra are expected to arise from a low-speed flyby: While the impact of olivine and LCP grains will produce spectra showing only a distinct Mg peak, HCP grain impacts will result in Ca and Mg-dominated spectra (+ potentially some Na and Al from augite in type 3 and 4 OCs; Brearley & Jones, 1998), whereas plagioclase grains exhibit simultaneous Ca, Na, and Al (without Mg), and the spectra from sulfide and FeNi-metal grain impacts will not show a clear peak signature. Although LCP may contain some Ca, the risk of misidentification is nevertheless estimated to be low, as the wollastonite content (of LCP) in all three groups does typically not

19455100, 2023, 10, Downloaded from https://onlinelibrary.wiley.com/doi/10.1111/maps.14060 by Freie Universitaet Berlin, Wiley Online Library on [16/10/2023]. See the Terms and Conditions (https://onlinelibrary.wiley.com/terms-and-conditions) on Wiley Online Library for rules of use; OA articles are governed by the applicable Creative Commons License

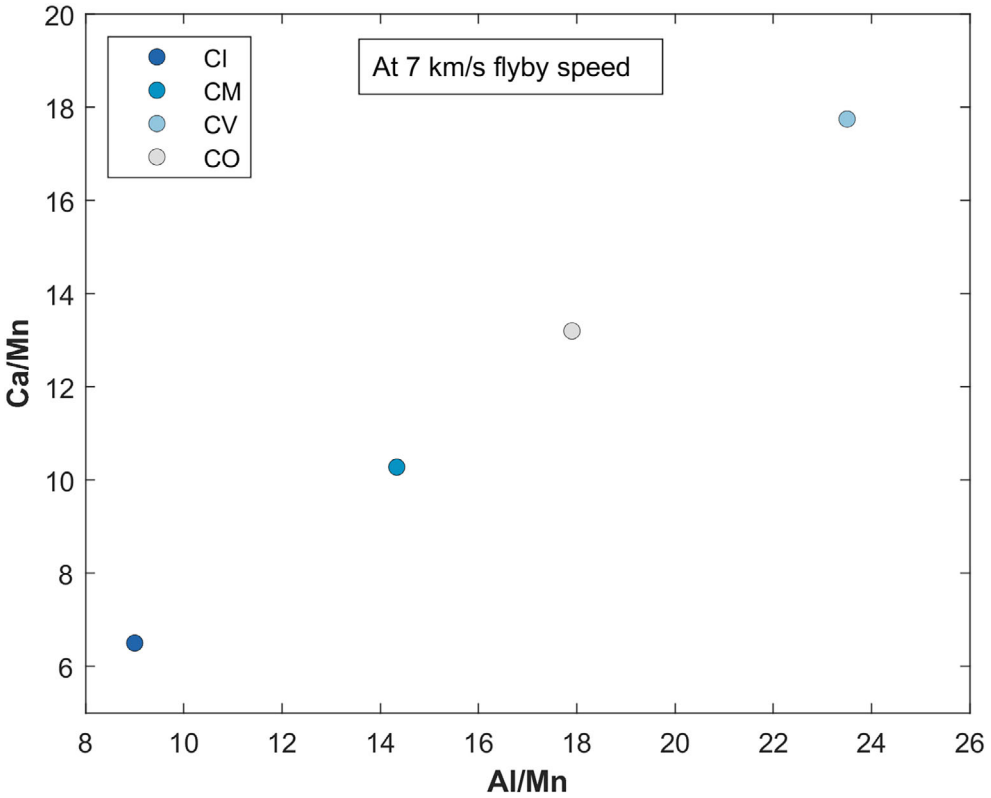

FIGURE 3. Separating CI, CM, CV, and COs at 7 km s^{-1} flyby speed using the bulk elemental ratios of Ca/Mn and Al/Mn (modified after Kalleymeyn & Wasson, 1981). (Color figure can be viewed at wileyonlinelibrary.com)

exceed 2 mole% (e.g., Artioli & Davoli, 1994; Slater-Reynolds & McSween Jr., 2005), therefore producing a spectrum strongly dominated by Mg. Consequently, a classification as H, L, or LL type may be possible based on the number of Mg-dominated spectra, deriving from olivine and LCP impacts, compared to the number of undistinctive spectra from FeNi-metal and sulfide grain impacts (Figure 4). It should be noted, however, that distinguishing between H and LL chondrites in a flyby of an H-analogue asteroid using the proportion of Mg-dominated spectra would require the detection of 585 grains for a 1-sigma identification, a number that is above the baseline assumption of this work.

With flybys at 9 km s^{-1} and above, we find that the groups of CCs, OCs and HEDs can be identified and discriminated between. In the case of the CCs, hydrated CI, CM, and CR chondrites can again be separated from (mostly) dry CV chondrites by means of their phyllosilicate abundances. The proportion of hydrated matrix material in CRs is typically smaller than in CIs and CMs, whilst exhibiting higher amounts of olivine (although there are some exceptions such as, for example, Al Rais and GRO 95577; Howard et al., 2015; that show similar properties to CM chondrites). These CC groups can thus be separated by comparing the frequency of spectra containing hydrated features with the amount of olivine grain impacts (Figure 5). Where necessary, the higher amounts of free metal in CRs (5–8 vol% FeNi-metal; e.g., Weisberg et al., 2006) may additionally aid in separating those from CMs and the different phyllosilicate mineralogy of CIs and CMs (saponite vs. serpentine) can be used to separate the two groups.

A similar classification scheme, distinguishing CM from CR chondrites based on the phyllosilicate fraction versus the total amount of olivine and pyroxene, was already proposed by Howard et al. (2015). However, we find that including pyroxene would not help to identify Al Rais and GRO 95577 as CR chondrites, and considering only olivine facilitates separating CVs from CRs, as the former is very olivine-rich, containing only minor pyroxene, while CRs are enriched in both.

As the OC groups, H, L, and LL, vary (decrease) in both total and free Fe, and Fe is an element known to be identifiable at intermediate flyby speeds of ≥9 km s^{-1}, the three groups can be distinguished by means of FeNi-metal grain abundance together with the Fe/Si ratio of the sum of the spectra (Figure 6) (average bulk Fe/Si atomic values and their ranges are taken from Van Schmus, 1969).

19455100, 2023, 10, Downloaded from https://onlinelibrary.wiley.com/doi/10.1111/maps.14060 by Freie Universitaet Berlin, Wiley Online Library on [16/10/2023]. See the Terms and Conditions (https://onlinelibrary.wiley.com/terms-and-conditions) on Wiley Online Library for rules of use; OA articles are governed by the applicable Creative Commons License

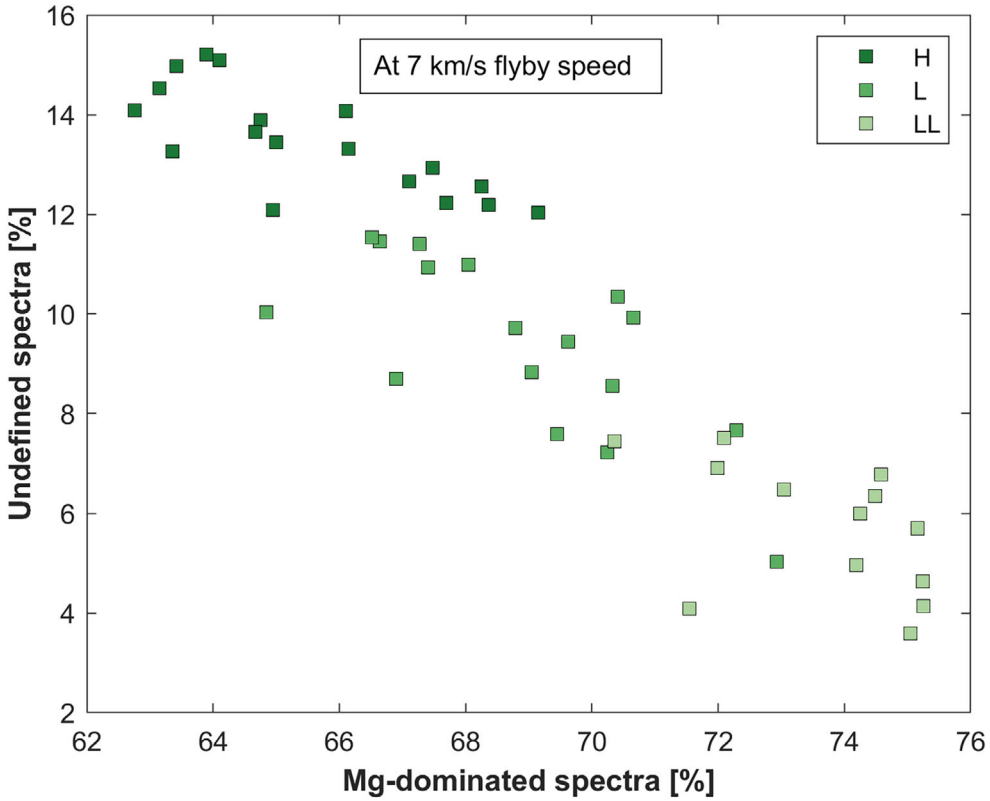

FIGURE 4. Discriminating between H, L, and LL ordinary chondrites at 7 km s^{-1} flyby speed based on the number of Mg-dominated spectra deriving from the impact of olivine and low-Ca pyroxene grains, compared to the number of spectra with no clear signature from the impact of FeNi-metal and sulfide grains. (Color figure can be viewed at wileyonlinelibrary.com)

DISCUSSION

For our approaches, it is vital that a sufficiently large number of dust grains detected during a flyby are monomineralic, which enables an individual mass spectrum to be assigned to a single mineral phase. This was also assumed by Cohen et al. (2019), who predicted dust grains to be monomineralic up to a size of 100 nm radius based on the Itokawa grain size/composition distribution determined by Nakamura et al. (2011), and extrapolation of grain composition with size from the Stardust collection (Brownlee et al., 2006; Hörz et al., 2006). Those returned samples were mostly micrometer-sized and multi-mineralic, but the proportion of single mineral grains increased at smaller grain sizes. A tendency towards grains with individual, homogeneous, compositions might be expected based upon the distribution of minerals within meteorites, and although it is possible that during regolith formation, there is melt or cohesive agglomeration of different composition grains, this does not seem to be the case for the smaller Itokawa samples. It can thus be assumed with confidence that also the smaller grain fraction (<100 nm) of the asteroid's dust shroud will be mostly of monomineralic compositions. Alternatively, the mass spectra from larger impacting multi-mineral grains could additionally be considered. This would require the identification of individual mineral phases from multi-mineral aggregates, which at the low speeds considered here is currently unproven and needs further investigation with laboratory dust detector calibration campaigns.

Furthermore, differences in space weathering, and excavation, mixing, or contamination of an asteroid's surface during impact events, may result in a divergence between the composition of ejected dust particles and meteorite compositions. Variations in ejecta yields, that is, the resistance of certain materials to fragmentation and spallation, may also bias the composition of the dust cloud of an asteroid. A range of experiments have been performed to determine the effect of hypervelocity impact comminution on meteorites. At larger scales, the size distribution of asteroidal regolith particles is expected to follow Rosin's Law (e.g., Deb & Sen, 2013), a relationship typically observed when materials are crushed. However, impact experiments with meteorites at smaller (microns to millimeters) scales, at which different strength regimes lie, indicate that chemical and mineralogical size segregation may occur. For example,

19455100, 2023, 10, Downloaded from https://onlinelibrary.wiley.com/doi/10.1111/maps.14060 by Freie Universitaet Berlin, Wiley Online Library on [16/10/2023]. See the Terms and Conditions (https://onlinelibrary.wiley.com/terms-and-conditions) on Wiley Online Library for rules of use; OA articles are governed by the applicable Creative Commons License

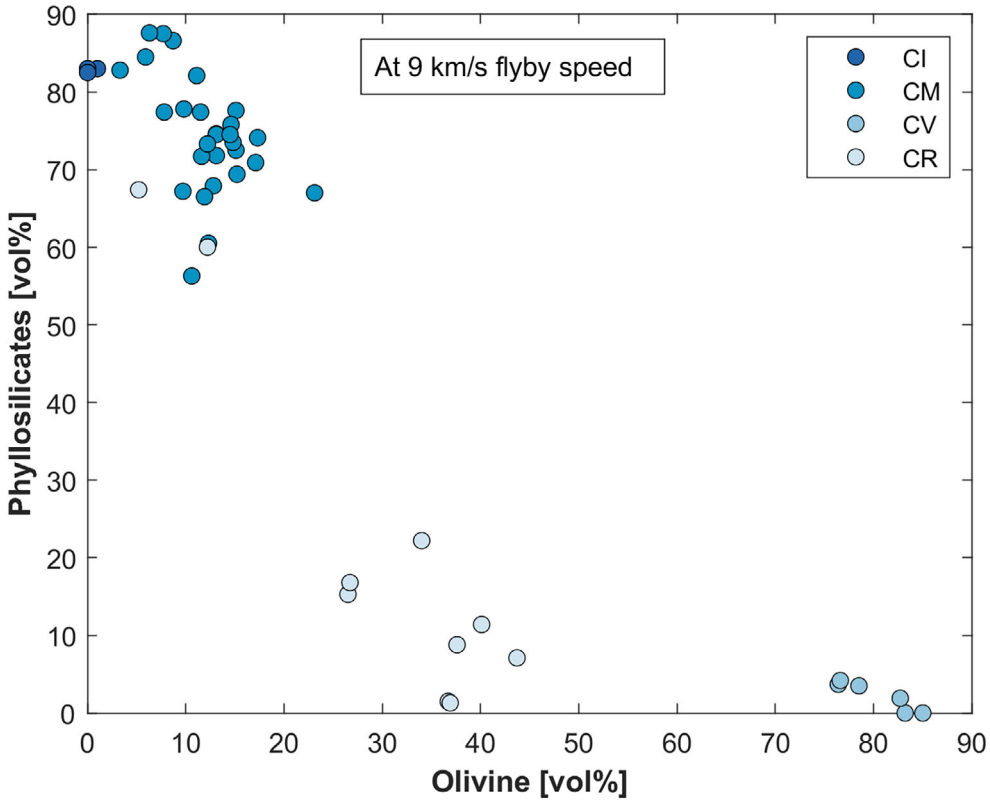

FIGURE 5. Discriminating between CI, CM, CV, and CR chondrites at 9 km s^{-1} flyby speed based on the phyllosilicate and olivine abundances. Phyllosilicates are recognized by the presence of water ion groups. The number of spectra from FeNi-metal grains may help to separate CIs and CMs from CRs, while a high number of spectra attributed to saponite would favor a CI-like composition. (Color figure can be viewed at wileyonlinelibrary.com)

L3-6 OCs were found to produce a small fragment (<30 μm) population overrepresented by matrix material, with larger (>30 μm) fragments more often composed of chondrule material (Flynn et al., 2018). Similarly, an increase in the Ni/Fe ratios of the smallest ejecta, compared with that >45 μm in size, produced by the impact disruption of eight anhydrous chondritic meteorites was observed by Flynn and Durda (2004). The analysis of an ensemble of spectra gathered during an asteroid flyby would necessarily need to take this compositional bias into account.

To date, the CC class recognizes eight different groups (plus the CL group recently proposed by Metzler et al., 2021). To conclude whether the separation of CCs is possible in the two flyby speed cases, our dataset needs to be extended to cover the whole range of bulk mineral volume abundances of CCs. For example, the abundant CO (Ornans-like) chondrites have very similar bulk mineral properties to CV chondrites. Both are mainly distinguished by different chondrule sizes (COs: mini-chondrule bearing (~150 μm; Rubin, 1989), while those in CVs are large (~1 mm; Weisberg et al., 2006), a parameter that may prove difficult to investigate with a dust instrument. However, we argue that it could still be possible to discriminate even such petrologically similar types at intermediate flyby speeds, using, in that case, the abundance of magnetite, the dominant oxide phase in CVs (0.3–6 vol%; Howard et al., 2010), which rarely occurs in COs. Including further CC groups may also influence some of the other classification schemes presented. For instance, CK chondrites are thermally metamorphosed and contain abundant plagioclase with large grain-to-grain variations (e.g., 13 vol% with $An_{27\text{-}76}$ in CK4 Kobe; Tomeoka et al., 2005; or see also Nogushi, 1993 for the plagioclase compositions of various CK chondrites), their compositions may overlap with those of OCs using the method from Figure 1. Where dust mass spectral analysis alone will not produce a conclusive result, additional constraints, such as data from spectroscopic observations, albedo or density may aid in classifying the asteroid's surface composition. Given that the reflectance spectra of CKs are darker than those of OCs, generally blue sloping, and in some cases exhibit a subdued 3 μm water-associated absorption feature (Cloutis et al., 2012; Miyamoto et al., 2018; Tanbakouei et al., 2021), the misidentification as an OC is rather unlikely.

19455100, 2023, 10, Downloaded from https://onlinelibrary.wiley.com/doi/10.1111/maps.14060 by Freie Universitaet Berlin, Wiley Online Library on [16/10/2023]. See the Terms and Conditions (https://onlinelibrary.wiley.com/terms-and-conditions) on Wiley Online Library for rules of use; OA articles are governed by the applicable Creative Commons License

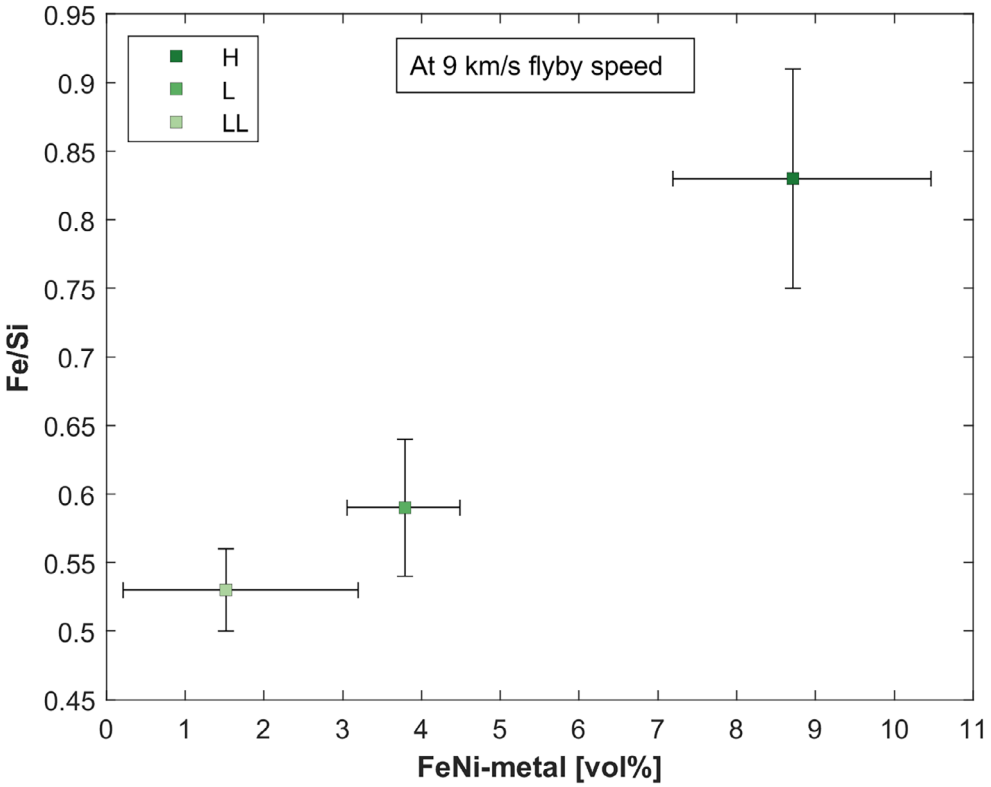

FIGURE 6. Discriminating between the ordinary chondrite groups, H, L, and LL at 9 km s^{-1} flyby speed by means of FeNi-metal abundance together with the Fe/Si ratio of the sum of the spectra. The bulk Fe/Si ratios and their ranges are extracted from Van Schmus (1969) as H: 0.83 ± 0.08, L: 0.59 ± 0.05, LL: 0.53 ± 0.03. (Color figure can be viewed at wileyonlinelibrary.com)

After Itokawa, the recent return of samples from asteroid Ryugu (C-type) by the Hayabusa2 mission and the foreseen return of samples from asteroid Bennu (B-type) by the OSIRIS-REx mission in 2023 provide unique opportunities to validate predicted asteroid-meteorite spectral matches from ground-based observations and establish new definite links. The reflectance spectra of both asteroids show similarities with CM chondrites but also feature properties similar to other chondrite groups (e.g., Hamilton et al., 2019; Le Corre et al., 2018; Merlin et al., 2021; Schröder et al., 2021). As with Itokawa, the returned samples can be used to determine the minimum number of monomineralic particles required to be detected during a flyby in order to identify a suitable meteorite analogue, if represented in the terrestrial collection. The outcome of those studies will allow us to verify the feasibility of the presented approaches beyond S-type asteroids and may build further confidence in those.

With the exception of water ion groups, we have so far mostly considered the detection of cations because anions, for example, F, Cl, and CN are impossible to reliably detect using a cation spectrometer. By using a dual-mode spectrometer, in which the detector is capable of switching between (or measuring simultaneously) two polarities, the number of dust grain impacts will need to be doubled to yield a suitable number of spectra for each channel. However, the ability to measure anions is important to detect organics, which would conclusively identify CCs and likely facilitate discriminating between CC groups (e.g., based on variations in the C/H ratio; see, for example, Alexander et al., 2013; Hirschmann, 2016; Jarosewich, 2006; Kerridge, 1985). Also, considering molecular ions within future studies, rather than focusing solely on elemental ones, will enhance the possibilities for discrimination, as for instance, laboratory impact experiments with polypyrrole-coated pyrrhotite microparticles by Hillier et al. (2014) indicate that detecting, for example, FeS^{+} may be possible already at lower impact speeds than their individual components, although detailed studies, especially using silicate minerals, the main components of meteorites, is required to verify this.

Flybys with encounter speeds above 10 km s^{-1} will increase the ion yield from impact ionization, increasing spectral signal strengths and enhancing the diagnostic capabilities presented here towards smaller particles. Since the number density in an ejecta cloud scales exponentially towards smaller particles (e.g., Szalay et al., 2018), an increase of a few km s^{-1} can easily double the number of sampled particles and with that, the accuracy

19455100, 2023, 10, Downloaded from https://onlinelibrary.wiley.com/doi/10.1111/maps.14060 by Freie Universitaet Berlin, Wiley Online Library on [16/10/2023]. See the Terms and Conditions (https://onlinelibrary.wiley.com/terms-and-conditions) on Wiley Online Library for rules of use; OA articles are governed by the applicable Creative Commons License

of the assessments shown here. Below ~15 km s^{-1}, water group ions would still not dissociate effectively into hydrogen and oxygen (e.g., Postberg et al., 2018) and could still be used to confidently identify hydroxyl as well as water constituents. Above approximately 15–20 km s^{-1}, oxygen cations effectively form (Fiege et al., 2014; Hillier et al., 2012; Postberg et al., 2009) and molecular constituents disintegrate. This high-speed regime is ideally suited to infer the elemental compositions of individual dust grains (e.g., Altobelli et al., 2016; Jessberger et al., 1988).

CONCLUSIONS AND OUTLOOK

Using previously published bulk mineral volume abundances—with an "ideal" detection limit of 1 vol%—we have shown theoretically that an ensemble of at least 100 grains detected by a dust mass spectrometer onboard a spacecraft flying at low-medium speeds (7–9 km s^{-1}) would allow the broad identification of the corresponding meteorite class, and to a certain extent, also the specific meteorite group of CCs, OCs and HED achondrites. As asteroid flyby speeds below 10 km s^{-1}will result in low-intermediate energy impacts of the dust grains onto the metal target of the detector, only elements that are easy to ionize, together with water group ions, are expected to be reliably detectable. The prediction and interpretation of spectra gathered during such flybys will need to take this velocity constraint into account.

Since many asteroids exhibit non-unique and often featureless reflectance spectra, remote sensing observations alone have, in many cases, proven insufficient to conclusively link asteroids and meteorites, highlighting the need for alternative, complementary methods. Particularly in the case of asteroids with non-diagnostic reflectance features (such as, e.g., C-, D-, B-, and X-type asteroids), in situ dust detection may provide a good complementary technique to establish new asteroid meteorite links, or—if flyby speeds are sufficiently high—to define new classes of parent bodies that currently cannot be linked to meteoritic classification schemes. This emphasizes the utility of dust instruments on future missions, especially to, or through, the main belt.

To extend the utility of our approaches, the dataset needs to include other meteorite classes and groups, particularly to identify further potential risks of misidentification between meteorite types not considered in this study. Also, publishing of available laboratory proof is yet required to show that spectra from, for example, olivine can be reliably distinguished from those of LCP, as well as confirm that OH and H_2O from hydrous minerals can be recognized in spectra gathered at 7–9 km s^{-1} impact speeds. By using a dust detector capable of switching between polarities, the more reliable identification of organics will be possible, thus providing a further compositional probe applicable to determining classes of CCs. Finally, accelerating samples of powdered meteorites, or suitably synthesized multi-mineral analog dust ensembles in future laboratory dust detector calibration campaigns would provide an excellent basis to interpret mineral spectra gathered during an asteroid flyby.

Conflict of Interest Statement—The authors declare that they have no competing financial or personal interests that could have influenced the work of this manuscript.

Acknowledgments—This work has been made possible by funding from Freie Universität Berlin, Germany, the German Research Foundation (DFG, grant #HI 2157/1-1), and the Swiss National Science Foundation (grant #200020_182649). We thank Jürgen Schmidt for helpful feedback to the manuscript. We thank Tomoko Arai and an anonymous referee for their helpful and constructive comments, which have improved the manuscript considerably. Open Access funding enabled and organized by Projekt DEAL.

Data Availability Statement—Data available on request from the authors.

Editorial Handling—Dr. Carle M. Pieters

REFERENCES

Alexander, C. M. O'D., Howard, K. T., Bowden, R., and Fogel, M. L. 2013. The Classification of CM and CR Chondrites Using Bulk H, C and N Abundances and Isotopic Compositions. *Geochimica et Cosmochimica Acta* 123: 244–260.

Altobelli, N., Postberg, F., Fiege, K., Trieloff, M., Kimura, H., Sterken, V. J., Hsu, H.-W., et al. 2016. Flux and Composition of Interstellar Dust at Saturn from Cassini's Cosmic Dust Analyzer. *Science* 352: 312–18.

Artioli, G., and Davoli, G. 1994. Low-Ca Pyroxenes from LL Group Chondritic Meteorites: Crystal Structural Studies and Implications for their Thermal Histories. *Earth and Planetary Science Letters* 128: 469–478.

Binzel, R. P., and Xu, S. 1993. Chips off of Asteroid 4 Vesta: Evidence for the Parent Body of Basaltic Achondrite Meteorites. *Science* 260: 186–191.

Brearley, A. J., and Jones, R. H. 1998. Chondritic Meteorites. In *Planetary Materials*, edited by J. Papike, Washington D.C.: Mineralogical Society of America.

Brownlee, D., Tsou, P., Aléon, J., Alexander, C. M. O'D., Araki, T., Bajt, S., Baratta, G., et al. 2006. Comet 81P/Wild 2 under a Microscope. *Science* 314: 1711–16.

Bus, S. J., Vilas, F., and Barucci, M. A. 2002. Visible-Wavelength Spectroscopy of Asteroids. In *Asteroids III*, edited by W. F. Bottke, Jr., A. Cellino, P. Paolicchi, and

19455100, 2023, 10, Downloaded from https://onlinelibrary.wiley.com/doi/10.1111/maps.14060 by Freie Universitaet Berlin, Wiley Online Library on [16/10/2023]. See the Terms and Conditions (https://onlinelibrary.wiley.com/terms-and-conditions) on Wiley Online Library for rules of use; OA articles are governed by the applicable Creative Commons License

R. P. Binzel, 169–182. Tucson, AZ: University of Arizona Press.
Carvano, J. M., Mothé-Diniz, T., and Lazzaro, D. 2003. Search for Relations Among a Sample of 460 Asteroids with Featureless Spectra. *Icarus* 161: 356–382.
Chapman, C. R. 1996. S-Type Asteroids, Ordinary Chondrites, and Space Weathering: The Evidence from Galileo's Fly-bys of Gaspra and Ida. *Meteoritics & Planetary Science* 31(6): 699–725. https://doi.org/10.1111/j.1945-5100.1996.tb02107.x.
Chapman, C. R. 2004. Space Weathering of Asteroid Surfaces. *Annual Review of Earth and Planetary Sciences* 32: 539–567. https://doi.org/10.1146/annurev.earth.32.101802.120453.
Cloutis, E. A., Gaffey, M. J., Smith, D. G. W., and Lambert, R. S. J. 1990. Reflectance Spectra of 'Featureless' Materials and the Surface Mineralogies of M- and E-Class Asteroids. *Journal of Geophysical Research* 95: 281–293.
Cloutis, E. A., Hudon, P., Hiroi, T., and Gaffey, M. J. 2012. Spectral Reflectance Properties of Carbonaceous Chondrites: 7. CK Chondrites. *Icarus* 221: 911–924.
Cloutis, E. A., Izawa, M. R. M., Pompilio, L., Reddy, V., Hiesinger, H., Nathues, A., Mann, P., Le Corre, L., Palomba, E., and Bell, J. F., III. 2013. Spectral Reflectance Properties of HED meteorites + CM2 Carbonaceous Chondrites: Comparison to HED Grain Size and Compositional Variations and Implications for the Nature of Low-Albedo Features on Asteroid 4 Vesta. *Icarus* 223(2): 850–877.
Cohen, B. A., Szalay, J. R., Rivkin, A. S., Richardson, J. A., Klima, R. L., Ernst, C. M., Chabot, N. L., Sternovsky, Z., and Horányi, M. 2019. Using Dust Shed from Asteroids as Microsamples to Link Remote Measurements with Meteorite Classes. *Meteoritics & Planetary Science* 54: 2046–66.
Deb, D., and Sen, A. K. 2013. Rosin's Law and Size Distribution of Particles in Regolith like Samples—An Analysis. *Planetary and Space Science* 82-83: 79–83.
DeMeo, F. E., Alexander, C. M. O'D., Walsh, K. J., Chapman, C. R., and Binzel, R. P. 2015. The Compositional Structure of the Asteroid Belt. In *Asteroids IV*, edited by P. Michel, F. E. DeMeo, and W. F. Bottke, 13–41. Tucson, AZ: University of Arizona Press.
DeMeo, F. E., Burt, B. J., Marsset, M., Polishook, D., Burbine, T. H., Carry, B., Binzel, R. P., et al. 2022. Connecting Asteroids and Meteorites with Visible and near-Infrared Spectroscopy. *Icarus* 380: 114971.
Drapatz, S., and Michel, K. W. 1974. Theory of Shock-Wave Ionization upon High-Velocity Impact of Micrometeorites. *Zeitschrift für Naturforschung A* 29: 870–79.
Dunn, T. L., Cressey, G., McSween, H. Y., Jr., and McCoy, T. J. 2010. Analysis of Ordinary Chondrites Using Powder X-Ray Diffraction: 1. Modal Mineral Abundances. *Meteoritics & Planetary Science* 45: 123–134.
Emery, J. P., Thomas, C. A., Reddy, V., and Moskovitz, N. A. 2019. Spectral Analyses of Asteroids. In *Remote Compositional Analysis: Techniques for Understanding Spectroscopy, Mineralogy, and Geochemistry of Planetary Surfaces*, edited by J. L. Bishop, J. F. Bell, III, and J. E. Moersch, 393–412. Cambridge: Cambridge University Press.
Farquhar, R. W., Kawaguchi, J., Russell, C. T., Schwehm, G., Veverka, J. F., and Yeomans, D. K. 2002. Spacecraft Exploration of Asteroids: The 2001 Perspective. In *Asteroids III*, edited by W. F. Bottke, Jr., A. Cellino, P. Paolicchi, and R. P. Binzel, 367–376. Tucson, AZ: University of Arizona Press.
Feierberg, M. A., Lebofsky, L. A., and Larson, H. P. 1981. Spectroscopic Evidence for Aqueous Alteration Products on the Surfaces of Low-Albedo Asteroids. *Geochimica et Cosmochimica Acta* 45: 971–981.
Fiege, K., Trieloff, M., Hillier, J. K., Guglielmino, M., Postberg, F., Srama, R., Kempf, S., and Blum, J. 2014. Calibration of Relative Sensitivity Factors for Impact Ionization Detectors with High-Velocity Silicate Microparticles. *Icarus* 241: 336–345.
Floran, R. J., Prinz, M., Hlava, P. F., Keil, K., Spettel, B., and Wänke, H. 1977. The Johnstown Orthopyroxenite (Diogenite) and its Relationship to Meteoritic Cumulates. *Meteoritics* 12: 226–27.
Floran, R. J., Prinz, M., Hlava, P. F., Keil, K., Spettel, B., and Wänke, H. 1981. Mineralogy, Petrology, and Trace Element Geochemistry of the Johnstown Meteorite: A Brecciated Orthopyroxenite with Siderophile and REE-Rich Components. *Geochimica et Cosmochimica Acta* 45 (12): 2385–91.
Flynn, G. J., and Durda, D. D. 2004. Chemical and Mineralogical Size Segregation in the Impact Disruption of Inhomogeneous, Anhydrous Meteorites. *Planetary and Space Science* 52: 1129–40.
Flynn, G. J., Durda, D. D., Patmore, E. B., Jack, S. J., Molesky, M. J., May, B. A., Congram, S. N., Strait, M. M., and Macke, R. J. 2018. Hypervelocity Cratering and Disruption of the Northwest Africa 869 Ordinary Chondrite Meteorite: Implications for Crater Production, Catastrophic Disruption, Momentum Transfer and Dust Production on Asteroids. *Planetary and Space Science* 164: 91–105.
Friichtenicht, J. F., and Slattery, J. C. 1963. Ionization Associated with Hypervelocity Impact. NASA Technical Note D-2091.
Fuhrman, M., and Papike, J. J. 1982. Howardites and Polymict Eucrites: Regolith Samples from the Eucrite Parent Body. Petrology of Bholghati, Bununu, Kapoeta, and ALHA76005, Proceedings 12th Lunar and Planetary Science Conference, Houston, TX, pp. 1257–79.
Gaffey, M. J. 2010. Space Weathering and the Interpretation of Asteroid Reflectance Spectra. *Icarus* 209: 564–574.
Gaffey, M. J., Burbine, T. H., and Binzel, R. P. 1993. Asteroid Spectroscopy: Progress and Perspectives. *Meteoritics* 28: 161–187.
Gilmour, I. 2003. 1.10—Structural and Isotopic Analysis of Organic Matter in Carbonaceous Chondrites. In *Treatise on Geochemistry*, edited by D. A. M. Pergamon, 269–290. Oxford: Elsevier.
Goode, W., Kempf, S., and Schmidt, J. 2021. Detecting the Surface Composition of Geological Features on Europa and Ganymede Using a Surface Dust Analyzer. *Planetary and Space Science* 208: 105343.
Greenwood, R. C., Burbine, T. H., and Franchi, I. A. 2020. Linking Asteroids and Meteorites to the Primordial Planetesimal Population. *Geochimica et Cosmochimica Acta* 277: 377–406.
Hamilton, V. E., Simon, A. A., Christensen, P. R., Reuter, D. C., Clark, B. E., Barucci, M. A., Bowles, N. E., et al. 2019. Evidence for Widespread Hydrated Minerals on Asteroid (101955) Bennu. *Nature Astronomy* 3: 332–340.
Hezel, D. C., Russell, S. S., Ross, A. J., and Kearsley, A. T. 2008. Modal Abundances of CAIs: Implications for Bulk

19455100, 2023, 10, Downloaded from https://onlinelibrary.wiley.com/doi/10.1111/maps.14060 by Freie Universitaet Berlin, Wiley Online Library on [16/10/2023]. See the Terms and Conditions (https://onlinelibrary.wiley.com/terms-and-conditions) on Wiley Online Library for rules of use; OA articles are governed by the applicable Creative Commons License

Chondrite Element Abundances and Fractionations. *Meteoritics & Planetary Science* 43: 1879–94.

Hillier, J. K., Postberg, F., Sestak, S., Srama, R., Kempf, S., Trieloff, M., Sternovsky, Z., and Green, S. F. 2012. Impact Ionization Mass Spectra of Anorthite Cosmic Dust Analogue Particles. *Journal of Geophysical Research: Planets* 117: E09002.

Hillier, J. K., Sternovsky, Z., Armes, S. P., Fielding, L. A., Postberg, F., Bugiel, S., Drake, K., Srama, R., Kearsley, A. T., and Trieloff, M. 2014. Impact Ionisation Mass Spectrometry of Polypyrrole-Coated Pyrrhotite Microparticles. *Planetary and Space Science* 97: 9–22.

Hillier, J. K., Sternovsky, Z., Kempf, S., Trieloff, M., Guglielmino, M., Postberg, F., and Price, M. C. 2018. Impact Ionisation Mass Spectrometry of Platinum-Coated Olivine and Magnesite-Dominated Cosmic Dust Analogues. *Planetary and Space Science* 156: 96–110.

Hinrichs, J. L., Lucey, P. G., Robinson, M. S., Meibom, A., and Krot, A. N. 1999. Implications of Temperature-Dependent Near-IR Spectral Properties of Common Minerals and Meteorites for Remote Sensing of Asteroids. *Geophysical Research Letters* 26: 1661–64.

Hiroi, T., and Pieters, C. M. 1992. Effects of Grain Size and Shape in Modeling Reflectance Spectra of Mineral Mixtures. Proceedings of the Lunar and Planetary Science Conference. Vol. 22, A92-30851 12-91, pp. 313–25

Hirschmann, M. M. 2016. Constraints on the Early Delivery and Fractionation of Earth's Major Volatiles from C/H, C/N, and C/S Ratios. *American Mineralogist* 101: 540–553.

Horányi, M., Szalay, J. R., Kempf, S., Schmidt, J., Grün, E., Srama, R., and Sternovsky, Z. 2015. A Permanent, Asymmetric Dust Cloud around the Moon. *Nature* 522: 324–26.

Hörz, F., Bastien, R., Borg, J., Bradley, J. P., Bridges, J. C., Brownlee, D. E., Burchell, M., et al. 2006. Impact Features on Stardust: Implications for Comet 81P/Wild 2 Dust. *Science* 314: 1716–19.

Howard, K. T., Alexander, C. M. O'D., Schrader, D. L., and Dyl, K. A. 2015. Classification of Hydrous Meteorites (CR, CM and C2 Ungrouped) by Phyllosilicate Fraction: PSD-XRD Modal Mineralogy and Planetesimal Environments. *Geochimica et Cosmochimica Acta* 149: 206–222.

Howard, K. T., Benedix, G. K., Bland, P. A., and Cressey, G. 2010. Modal Mineralogy of CV3 Chondrites by X-Ray Diffraction (PSD-XRD). *Geochimica et Cosmochimica Acta* 74: 5084–97.

Jarosewich, E. 2006. Chemical Analyses of Meteorites at the Smithsonian Institution: An Update. *Meteoritics & Planetary Science* 41: 1381–82.

Jessberger, E. K., Christoforidis, A., and Kissel, J. 1988. Aspects of the Major Element Composition of Hally's Dust. *Nature* 332: 691–95.

Kallemeyn, G. W., and Wasson, J. T. 1981. The Compositional Classification of Chondrites—I. The Carbonaceous Chondrite Groups. *Geochimica et Cosmochimica Acta* 45: 1217–30.

Kempf, S., Altobelli, N., Briois, C., Grün, E., Horanyi, M., Postberg, F., Schmidt, J., Srama, R., Sternovsky, Z., and Tobie, G. 2014. SUDA: A Dust Mass Spectrometer for Compositional Surface Mapping for a Mission to Europa International Workshop on Instrumentation for Planetary Missions, p. 7.

Kerridge, J. F. 1985. Carbon, Hydrogen and Nitrogen in Carbonaceous Chondrites: Abundances and Isotopic Compositions in Bulk Samples. *Geochimica et Cosmochimica Acta* 49: 1707–14.

King, A. J., Schofield, P. F., Howard, K. T., and Russell, S. S. 2015. Modal mineralogy of CI and CI-like chondrites by X-ray diffraction. *Geochimica et Cosmochimica Acta* 165: 148–160.

Kitts, K., and Lodders, K. 1998. Survey and Evaluation of Eucrite Bulk Compositions. *Meteoritics & Planetary Science* 33: A197–A213.

Kovach, H. A., and Jones, R. H. 2010. Feldspar in Type 4–6 Ordinary Chondrites: Metamorphic Processing on the H and LL Chondrite Parent Bodies. *Meteoritics & Planetary Science* 45: 246–264.

Krüger, H., Krivov, A. V., and Grün, E. 2000. A Dust Cloud of Ganymede Maintained by Hypervelocity Impacts of Interplanetary Micrometeoroids. *Planetary and Space Science* 48: 1457–71.

Krüger, H., Krivov, A. V., Hamilton, D. P., and Grün, E. 1999. Detection of an Impact-Generated Dust Cloud around Ganymede. *Nature* 399: 558–560.

Le Bras, A., and Erard, S. 2003. Reflectance Spectra of Regolith Analogs in the Mid-Infrared: Effects of Grain Size. *Planetary and Space Science* 51: 281–294.

Le Corre, L., Sanchez, J. A., Reddy, V., Takir, D., Cloutis, E. A., Thirouin, A., Becker, K. J., Li, J.-Y., and Tatsumi, E. 2018. Ground-Based Characterization of Hayabusa2 Mission Target Asteroid 162173 Ryugu: Constraining Mineralogical Composition in Preparation for Spacecraft Operations. *Monthly Notices of the Astronomical Society* 475: 614–623.

Li, J.-Y., Helfenstein, P., Buratti, B. J., Takir, D., and Clark, B. E. 2015. Asteroid Photometry. In *Asteroids IV*, edited by P. Michel, F. E. DeMeo, and W. F. Bottke, 129–150. Tucson, AZ: University of Arizona Press.

Li, S., and Milliken, R. E. 2015. Estimating the Modal Mineralogy of Eucrite and Diogenite Meteorites Using Visible–Near Infrared Reflectance Spectroscopy. *Meteoritics & Planetary Science* 50(11): 1821–50.

Licandro, J., Alvarez-Candal, A., León, J. D., Pinilla-Alonso, N., Lazzaro, D., and Campins, H. 2008. Spectral Properties of Asteroids in Cometary Orbits. *Astronomy and Astrophysics* 481: 861–877.

MacPherson, G. J. 2014. Calcium-Aluminum-Rich Inclusions in Chondritic Meteorites. In *Meteorites and Cosmochemical Processes*, edited by A. M. Davis, Vol. 1 Treatise on Geochemistry, 2nd ed., H. D. Holland and K. K. Turekian, executive editors, 139–79. Oxford: Elsevier.

May, C., Russell, S. S., and Grady, M. M. 1999. Analysis of Chondrule and CAI Size and Abundance in CO3 and CV3 Chondrites: A Preliminary Study. 30th Annual Lunar and Planetary Science Conference, abstract #1688.

McComas, D. J., Christian, E. R., Schwadron, N. A., Fox, N., Westlake, J., Allegrini, F., Baker, D. N., et al. 2018. Interstellar Mapping and Acceleration Probe (IMAP): A New NASA Mission. *Space Science Reviews* 214: 27–54.

McCord, T. B., Adams, J. B., and Johnson, T. V. 1970. Asteroid Vesta: Spectral Reflectivity and Compositional Implications. *Science* 168: 1445–47.

McSween, H. Y. 1977. Chemical and Petrographic Constraints on the Origin of Chondrules and Inclusions in Carbonaceous Chondrites. *Geochimica et Cosmochimica Acta* 41: 1843–60.

McSween, H. Y., and Binzel, R. P. 2022. Protoplanet Vesta and HED Meteorites. In *Vesta and Ceres: Insights from*

19455100, 2023, 10, Downloaded from https://onlinelibrary.wiley.com/doi/10.1111/maps.14060 by Freie Universitaet Berlin, Wiley Online Library on [16/10/2023]. See the Terms and Conditions (https://onlinelibrary.wiley.com/terms-and-conditions) on Wiley Online Library for rules of use; OA articles are governed by the applicable Creative Commons License

the Dawn Mission for the Origin of the Solar System, edited by S. Marchi, C. A. Raymond, and C. T. Russell, 41–52. Cambridge: Cambridge University Press.

Merlin, F., Deshapriya, J. D. P., Fornasier, S., Barucci, M. A., Praet, A., Hasselmann, P. H., Clark, B. E., et al. 2021. Search of Bennu Analogs: Hapke Modeling of Meteorite Mixtures. *Astronomy & Astrophysics* 648: A88.

Metzler, K., Hezel, D. C., Barosch, J., Wölfer, E., Schneider, J. M., Hellmann, J. L., Berndt, J., et al. 2021. The Loongana (CL) Group of Carbonaceous Chondrites. *Geochimica et Cosmochimica Acta* 304: 1–31.

Miyamoto, H., Hong, P. K., Niihara, T., Kuritani, T., Fukumizu, K., Hino, H., Nagata, K., et al. 2018. Reflectance Spectra of Asteroids and Meteorites: Their Classifications and Statistical Comparisons. *Journal of Physics: Conference Series* 1036: 012003.

Miyamoto, M., and Takeda, H. 1994. Evidence for Excavation of Deep Crustal Material of a Vesta-Like Body from Ca Compositional Gradients in Pyroxene. *Earth and Planetary Science Letters* 122: 343–49.

Mocker, A., Hornung, K., Grün, E., Kempf, S., Collette, A., Drake, K., Horányi, M., Munsat, T., O'Brien, L., and Sternovsky, Z. 2013. On the Application of a Linear Time-of-Flight Mass Spectrometer for the Investigation of Hypervelocity Impacts of Micron and Sub-Micron Sized Dust Particles. *Planetary and Space Science* 89: 47–57.

Moroz, L., Schade, U., and Wäsch, R. 2000. Reflectance Spectra of Olivine–Orthopyroxene-Bearing Assemblages at Decreased Temperatures: Implications for Remote Sensing of Asteroids. *Icarus* 147: 79–93.

Nakamura, T., Noguchi, T., Tanaka, M., Zolensky, M. E., Kimura, M., Tsuchiyama, A., Nakato, A., et al. 2011. Itokawa Dust Particles: A Direct Link between S-Type Asteroids and Ordinary Chondrites. *Science* 333: 1113–16.

Nakamuta, Y., and Motomura, Y. 1999. Sodic Plagioclase Thermometry of Type 6 Ordinary Chondrites: Implications for the Thermal Histories of Parent Bodies. *Meteoritics & Planetary Science* 34: 763–772.

Nogushi, T. 1993. Petrology and Mineralogy of CK Chondrites: Implications for the Metamorphism of the CK Chondrite Parent Body. *Proceedings of the NIPR Symposium on Antarctic Meteorites* 6: 204–233.

Norton, M. B., and McSween, H. Y. 2007. Quantifying the Volumetric Abundances of the Components of the Murray CM Chondrite: A Preliminary Investigation. 38th Lunar and Planetary Science Conference, abstract #1338.

Pieters, C. M., and McFadden, L. A. 1994. Meteorite and Asteroid Reflectance Spectroscopy: Clues to Early Solar System Processes. *Annual Review of Earth and Planetary Sciences* 22: 457–497.

Pieters, C. M., Taylor, L. A., Noble, S. K., Keller, L. P., Hapke, B., Morris, R. V., Allen, C. C., McKay, D. S., and Wentworth, S. 2000. Space Weathering on Airless Bodies: Resolving a Mystery with Lunar Samples. *Meteoritics & Planetary Science* 35: 1101–7.

Pokorný, P., Janches, D., Sarantos, M., Szalay, J. R., Horányi, M., Nesvorný, D., and Kuchner, M. J. 2019. Meteoroids at the Moon: Orbital Properties, Surface Vaporization, and Impact Ejecta Production. *Journal of Geophysical Research: Planets* 124: 752–778.

Postberg, F., Grün, E., Horanyi, M., Kempf, S., Krüger, H., Schmidt, J., Spahn, F., Srama, R., Sternovsky, Z., and Trieloff, M. 2011. Compositional Mapping of Planetary Moons by Mass Spectrometry of Dust Ejecta. *Planetary and Space Science* 59: 1815–25.

Postberg, F., Kempf, S., Rost, D., Stephan, T., Srama, R., Trieloff, M., Mocker, A., and Goerlich, M. 2009. Discriminating Contamination from Particle Components in Spectra of Cassini's Dust Detector CDA. *Planetary and Space Science* 57: 1359–74.

Postberg, F., Khawaja, N., Abel, B., Choblet, G., Glein, C. R., Gudipati, M. S., Henderson, B. L., et al. 2018. Macromolecular Organic Compounds from the Depths of Enceladus. *Nature* 558: 564–68.

Reddy, V., Dunn, T. L., Thomas, C. A., Moskovitz, N. A., and Burbine, T. H. 2015. Mineralogy and Surface Composition of Asteroids. In *Asteroids IV*, edited by P. Michel, F. E. DeMeo, and W. F. Bottke, 43–63. Tucson, AZ: University of Arizona Press.

Rubin, A. E. 1989. Size-Frequency Distributions of Chondrules in CO3 Chondrites. *Meteoritics* 24: 179–189.

Rubin, A. E. 1997. Mineralogy of Meteorite Groups. *Meteoritics & Planetary Science* 32: 231–247.

Rubin, A. E. 2015. An American on Paris: Extent of Aqueous Alteration of a CM Chondrite and the Petrography of its Refractory and Amoeboid Olivine Inclusions. *Meteoritics & Planetary Science* 50: 1595–1612.

Schröder, S., Otto, K., Scharf, H., Matz, K.-D., Schmitz, N., Scholten, F., Mottola, S., Trauthan, F., Koncz, A., and Michaelis, H. 2021. Spectrophotometric Analysis of the Ryugu Rock Seen by MASCOT: Searching for a Carbonaceous Chondrite Analog. *The Planetary Science Journal* 2: 2.

Schwartz, J. M., and McCallum, I. S. 2001. Evolution of the Basaltic Eucrite, Haraiya 6277. 32nd Annual Lunar and Planetary Science Conference, abstract no #2030.

Slater-Reynolds, V., and McSween, H. Y., Jr. 2005. Peak Metamorphic Temperatures in Type 6 Ordinary Chondrites: An Evaluation of Pyroxene and Plagioclase Geothermometry. *Meteoritics & Planetary Science* 40: 745–754.

Srama, R., Ahrens, T. J., Altobelli, N., Auer, S., Bradley, J. G., Burton, M., Dikarev, V. V., et al. 2004. The Cassini Cosmic Dust Analyzer. In *The Cassini-Huygens Mission: Orbiter In Situ Investigations*, edited by C. T. Russell, 2nd ed., 465–518. Dordrecht: Springer.

Srama, R., Kobayashi, M., Krüger, H., Arai, T., Kimura, H., Trieloff, M., Agarwal, J., Li, Y., Postberg, F., and Khawaja, N. 2019. Dust Astronomy with DESTINY PLUS at 1 AU. *Geophysical Research Abstracts* 21: p1-1 1p.

Szalay, J. R., and Horányi, M. 2016. The Impact Ejecta Environment of near Earth Asteroids. *The Astrophysical Journal* 830: L29.

Szalay, J. R., Poppe, A. R., Agarwal, J., Britt, D. T., Belskaya, I., Horányi, M., Nakamura, T., Sachse, M., and Spahn, F. 2018. Dust Phenomena Relating to Airless Bodies. *Space Science Reviews* 214: 1–47.

Tanbakouei, S., Trigo-Rodríguez, J. M., Llorca, J., Moyano-Cambero, C. E., Williams, I. P., and Rivkin, A. S. 2021. The Reflectance Spectra of CV–CK Carbonaceous Chondrites from the Near-Infrared to the Visible. *Monthly Notices of the Royal Astronomical Society* 507: 651–662.

Tomeoka, K., Kojima, T., Ohnishi, I., Ishii, Y., and Nakamura, N. 2005. The Kobe CK Carbonaceous Chondrite: Petrography, Mineralogy and Metamorphism.

19455100, 2023, 10, Downloaded from https://onlinelibrary.wiley.com/doi/10.1111/maps.14060 by Freie Universitaet Berlin, Wiley Online Library on [16/10/2023]. See the Terms and Conditions (https://onlinelibrary.wiley.com/terms-and-conditions) on Wiley Online Library for rules of use; OA articles are governed by the applicable Creative Commons License

Journal of Mineralogical and Petrological Sciences 100: 116–125.

Van Schmus, W. R. 1969. The Mineralogy and Petrology of Chondritic Meteorites. *Earth-Science Reviews* 5: 145–184.

Weisberg, M. K., Mccoy, T. J., and Krot, A. N. 2006. Systematics and Evaluation of Meteorite Classification. In *Meteorites and the Early Solar System II*, edited by D. S. Lauretta, and H. McSween, 19–52. Tucson, AZ: University of Arizona Press.

Wylie, C. C. 1939. Where Do Meteorites Come from? *Science* 90: 264–65.

Zolensky, M., Barrett, R., and Browning, L. 1993. Mineralogy and Composition of Matrix and Chondrule Rims in Carbonaceous Chondrites. *Geochimica et Cosmochimica Acta* 57: 3123–48.

19455100, 2023, 10, Downloaded from https://onlinelibrary.wiley.com/doi/10.1111/maps.14060 by Freie Universitaet Berlin, Wiley Online Library on [16/10/2023]. See the Terms and Conditions (https://onlinelibrary.wiley.com/terms-and-conditions) on Wiley Online Library for rules of use; OA articles are governed by the applicable Creative Commons License

APPENDIX A

TABLE A1. Bulk mineral volume abundances of the meteorites used in this study.

Sample	Group	Olivine	Low-Ca pyroxene	High-Ca pyroxene	Plagioclase	Phyllosilicates	Sulfide	FeNi-metal	Magnetite	Ferrihydrite	Carbonates	Gypsum	Other[a]	Reference
CI chondrites														
Orgueil	CI1	1				83	5.7		6.7	3.3		0.3		[1]
Alais	CI1	0				83	4		7	3	3			[1]
Ivuna	CI1	0				82.5	6.5		9		2			[1]
CM chondrites														
QUE 97990	CM2	23.1				67	0.9	0.2	0.6		0.9			[2]
Y791198	CM2	17.1				70.9	0.6	0.2	0.7		1			[2]
Murchison (n = 2)	CM2	15.1				72.5	1.8	0	1.1		1.2			[2]
Murray	CM2	17.3				74.1	1.8	n.d.	1.4		n.d.			[2]
Mighei (n = 3)	CM2	13.1				74.6	1.9	n.d.	2.3		1.2			[2]
ALHA 81002	CM2	15.1				77.6	1.4	n.d.	1.3		n.d.			[2]
Nogoya (n = 2)	CM2	14.6				75.8	2.3	n.d.	2.2		1.1			[2]
Nogoya	CM2	5.9				84.5	2.3	n.d.	5.3		2			[2]
Cold Bokkeveld (n = 2)	CM2	11.5				77.4	3	n.d.	2		1	0.8		[2]
QUE 93005 (n = 2)	CM2	11.1				82.1	2.2	n.d.	1.5		1.7			[2]
LON 94102	CM2	7.8				77.4	5.4	n.d.	2.4		1.1	2.2		[2]
ALH 85013	CM2	9.8				77.8	1.6	n.d.	1.6		4	1.9		[2]
LEW 88001	CM2	13.1				71.8	2.9	n.d.	1.9		3			[2]
LEW 90500	CM2	15.2				69.4	3.1	n.d.	1.9		1	3.7		[2]
TIL 91722	CM2	12.3				60.5	0.9	n.d.	1.9		3.9	9.3		[2]
DOM 09013	CM2	12.8				67.9	1.6	n.d.	0.3		3.4			[2]
LAP 03718	CM2	9.7				67.2	1.7	0.2	2.2		1.1			[2]
MAC 88101	CM2	13.1				74.5	1.5	n.d.	2.5		2.8			[2]
DNG 06004	CM2	10.6				56.3	2.2	n.d.	4		3.4			[2]
LAP 02336	CM2	11.6				71.7	1.6	0.4	1.3		4.2			[2]
MET 00432	CM2	3.3				82.8	2.2	n.d.	8.4		n.d.			[2]
LAP 02333	CM2	12.2				73.3	1.4	n.d.	1.8		0.9			[2]
ALH 83100	CM2/1	8.7				86.6	1	n.d.	1.7		1.2			[2]
MET 01070	CM1	7.7				87.5	1.2	n.d.	1.8		1.9			[2]
SCO 06043	CM1	6.3				87.6	2.7	n.d.	1.6		1.7			[2]
WIS 96100	C2ung	14.8				73.5	3.5		6.5		n.d.			[2]
Essebi	CM2/C2ung	14.5				74.5	3.9		5.2		0.8			[2]
Bells	CM2/C2ung	11.9				66.5	11.6		4.5		1.7			[2]
CV chondrites														
Vigarano	CV3	85	8.1		1.1	n.d.	2.4	2	1.4					[3]
Effremovka	CV3	83.2	6.5		1.2	n.d.	5.1	2.2	1.8					[3]

TABLE A1. *Continued.* Bulk mineral volume abundances of the meteorites used in this study.

Sample	Group	Olivine	Low-Ca pyroxene	High-Ca pyroxene	Plagioclase	Phyllosilicates	Sulfide	FeNi-metal	Magnetite	Ferrihydrite	Carbonates	Gypsum	Other[a]	Reference
Mokoia	CV3	76.4	6.3		1.7	3.7	8.1	1.1	2.6					[3]
Grosnaja	CV3	76.6	4.8		1.3	4.2	7.9	0.8	4.3					[3]
Kaba	CV3	78.5	7.8		1.1	3.5	2.9	0.2	6.1					[3]
Allende	CV3	82.7	6.3		1.1	1.9	6.6	1	0.3					[3]
CR chondrites														
PCA 91082	CR2	26.5				15.3	4.7	3.6	n.d.		n.d.			[2]
GRA 95229	CR2	37.6				8.8	3.2	6.2	n.d.		n.d.			[2]
LAP 02342	CR2	43.7				7.1	3.4	7.1	n.d.		n.d.			[2]
QUE 99177	CR3	36.7				1.5	5.3	5.6	0.9		n.d.			[2]
MET 00426	CR3	36.9				1.3	3.5	4.2	0.2		n.d.			[2]
GRA 06100	CR2	40.1				11.4	7.1	2.7	0.2		n.d.			[2]
GRO 03116	CR2	26.7				16.8	4.4	3.6	0.2		n.d.			[2]
AL Rais	CR2	12.2				60	6.1	5	10.9		n.d.			[2]
GRO 95577	CR1	5.2				67.4	9.3	n.d.	7		5.7			[2]
Dhofar 1432	CR2	34				22.2	5.9	0.2	0.5		n.d.			[2]
Ordinary chondrites														
Farmville	H4	*34.14*	*30.86*	*8.24*	*11.90*		*4.59*	*8.86*					*1.42*	[4]
Forest Vale	H4	*34.63*	*28.80*	*8.19*	*11.87*		*4.51*	*10.47*					*1.54*	[4]
Kabo	H4	*33.05*	*30.10*	*7.43*	*13.37*		*5.12*	*9.41*					*1.52*	[4]
Marilia	H4	*33.52*	*31.24*	*7.06*	*12.88*		*4.92*	*8.97*					*1.42*	[4]
Sao Jose do Rio Preto	H4	*33.57*	*29.19*	*8.88*	*12.85*		*5.57*	*8.52*					*1.42*	[4]
Allegan	H5	*34.38*	*29.71*	*7.91*	*11.37*		*5.48*	*9.62*					*1.53*	[4]
Ehole	H5	*38.88*	*28.82*	*7.65*	*11.02*		*3.75*	*8.48*					*1.41*	[4]
Itapicuru-Mirim	H5	*37.69*	*26.20*	*6.94*	*12.52*		*4.83*	*10.37*					*1.44*	[4]
Lost City	H5	*35.31*	*28.04*	*8.01*	*13.79*		*4.41*	*8.85*					*1.59*	[4]
Pribram	H5	*36.19*	*28.48*	*8.30*	*11.97*		*5.70*	*7.95*					*1.41*	[4]
Schenectady	H5	*39.90*	*27.21*	*6.67*	*12.07*		*4.63*	*8.03*					*1.50*	[4]
Uberaba	H5	*38.36*	*26.59*	*8.83*	*12.75*		*4.90*	*7.19*					*1.39*	[4]
Andura	H6	*40.05*	*29.11*	*5.43*	*11.82*		*4.74*	*7.29*					*1.57*	[4]
Butsura	H6	*38.34*	*30.02*	*6.38*	*11.46*		*3.35*	*8.84*					*1.59*	[4]
Canon City	H6	*39.64*	*26.46*	*6.54*	*11.68*		*5.02*	*9.05*					*1.60*	[4]
Chiang Khan	H6	*37.04*	*30.44*	*6.21*	*12.02*		*4.69*	*8.24*					*1.36*	[4]
Guaerena	H6	*44.64*	*23.61*	*5.06*	*12.63*		*3.90*	*8.66*					*1.50*	[4]
Ipiranga	H6	*38.36*	*27.78*	*6.78*	*12.35*		*5.28*	*8.04*					*1.41*	[4]
Atarra	L4	*42.75*	*22.09*	*11.03*	*12.75*		*6.07*	*3.96*					*1.35*	[4]
Bald Mountain	L4	*41.36*	*25.27*	*8.39*	*12.16*		*6.97*	*4.49*					*1.36*	[4]
Rio Negro	L4	*44.21*	*26.04*	*8.61*	*12.52*		*3.59*	*3.62*					*1.41*	[4]
Rupota	L4	*45.02*	*25.31*	*8.03*	*11.67*		*4.91*	*3.64*					*1.41*	[4]
Ausson	L5	*41.00*	*25.90*	*7.34*	*15.82*		*4.23*	*4.46*					*1.25*	[4]
Blackwell	L5	*46.45*	*26.48*	*9.62*	*11.12*		*1.97*	*3.05*					*1.31*	[4]
Cilimus	L5	*46.52*	*25.77*	*6.87*	*11.85*		*4.27*	*3.39*					*1.32*	[4]
Guibga	L5	*43.96*	*23.32*	*8.27*	*11.87*		*7.11*	*4.29*					*1.18*	[4]

19455100, 2023, 10, Downloaded from https://onlinelibrary.wiley.com/doi/10.1111/maps.14060 by Freie Universitaet Berlin, Wiley Online Library on [16/10/2023]. See the Terms and Conditions (https://onlinelibrary.wiley.com/terms-and-conditions) on Wiley Online Library for rules of use; OA articles are governed by the applicable Creative Commons License

TABLE A1. *Continued.* Bulk mineral volume abundances of the meteorites used in this study.

Sample	Group	Olivine	Low-Ca pyroxene	High-Ca pyroxene	Plagioclase	Phyllosilicates	Sulfide	FeNi-metal	Magnetite	Ferrihydrite	Carbonates	Gypsum	Other[a]	Reference
Mabwe-Khoyawa	L5	*44.80*	*25.85*	*6.23*	*11.86*		*6.40*	*3.52*					*1.34*	[4]
Malakal	L5	*44.53*	*24.26*	*8.30*	*12.02*		*5.73*	*3.99*					*1.17*	[4]
Messina	L5	*45.86*	*24.55*	*8.64*	*9.34*		*6.76*	*3.59*					*1.26*	[4]
Apt	L6	*42.72*	*23.80*	*8.42*	*12.18*		*7.99*	*3.54*					*1.34*	[4]
Aumale	L6	*45.43*	*22.62*	*8.04*	*11.58*		*6.93*	*4.05*					*1.35*	[4]
Karkh	L6	*46.14*	*23.48*	*7.98*	*11.61*		*5.56*	*3.89*					*1.34*	[4]
Kunashak	L6	*46.35*	*22.70*	*7.72*	*13.07*		*5.37*	*3.46*					*1.33*	[4]
Kyushu	L6	*46.34*	*21.07*	*8.42*	*12.05*		*7.22*	*3.72*					*1.18*	[4]
New Concord	L6	*47.11*	*22.34*	*8.92*	*12.79*		*3.83*	*3.76*					*1.24*	[4]
Benares (a)	LL4	*47.79*	*23.75*	*9.46*	*13.65*		*3.87*	*0.21*					*1.26*	[4]
Greenwell Springs	LL4	*52.24*	*22.34*	*6.37*	*11.05*		*4.89*	*1.89*					*1.22*	[4]
Hamlet	LL4	*50.94*	*23.25*	*7.17*	*12.39*		*3.49*	*1.48*					*1.29*	[4]
Witsand Farm	LL4	*53.06*	*21.43*	*6.83*	*11.03*		*3.19*	*3.15*					*1.32*	[4]
Aldsworth	LL5	*53.78*	*21.38*	*6.55*	*11.28*		*3.60*	*2.11*					*1.30*	[4]
Alat'ameem	LL5	*51.98*	*23.27*	*7.73*	*11.11*		*3.77*	*0.86*					*1.28*	[4]
Olivenza	LL5	*52.23*	*22.02*	*6.70*	*11.69*		*4.69*	*1.31*					*1.37*	[4]
Paragould	LL5	*51.59*	*20.40*	*6.73*	*13.06*		*3.72*	*3.20*					*1.32*	[4]
Tuxtuac	LL5	*52.50*	*22.54*	*7.69*	*12.40*		*2.65*	*0.95*					*1.27*	[4]
Bandong	LL6	*51.64*	*18.71*	*7.39*	*13.43*		*6.40*	*1.05*					*1.37*	[4]
Cherokee Spring	LL6	*52.77*	*19.32*	*6.54*	*12.63*		*6.07*	*1.45*					*1.22*	[4]
Karatu	LL6	*57.79*	*17.46*	*7.97*	*11.53*		*3.45*	*0.69*					*1.11*	[4]
Saint-Severin	LL6	*52.76*	*20.29*	*7.32*	*11.86*		*5.08*	*1.40*					*1.30*	[4]
HED														
Bholghati	Howardite	2	39	26	20.5								4	[5]
NWA 1942	Howardite	*0.94*	*58.35*	n.d.	*40.71*		n.d.							[6]
NWA1943	Howardite	n.d.	*37.59*	*13.58*	*48.83*		n.d.							[6]
NWA 5751	Howardite	*0.97*	*58.52*	*6.72*	*33.72*		n.d.						*0.07*	[6]
JaH 626	Shocked polymict eucrite	n.d.	*53.83*	n.d.	*45.52*		n.d.						*0.64*	[6]
Millbillillie	Polymict eucrite	n.d.	*33.56*	*10.73*	*54.95*		*0.07*						*0.70*	[6]
NWA 1836	Cumulate monomict eucrite	n.d.	*67.04*	n.d.	*32.89*		n.d.						*0.07*	[6]
NWA 6477	Eucrite	n.d.	*29.08*	*11.39*	*59.35*		*0.06*						*0.12*	[6]
Talampaya	Cumulate eucrite	n.d.	*27.68*	*0.86*	*70.12*		*0.06*						*1.28*	[6]
Haraiya	Eucrite		55	5	40								1	[7]
ALHA 81001	Eucrite		33.79	8.671	61									[8]
BTN 00300	Eucrite		34.17	11.50	48.00									[8]

19455100, 2023, 10, Downloaded from https://onlinelibrary.wiley.com/doi/10.1111/maps.14060 by Freie Universitaet Berlin, Wiley Online Library on [16/10/2023]. See the Terms and Conditions (https://onlinelibrary.wiley.com/terms-and-conditions) on Wiley Online Library for rules of use; OA articles are governed by the applicable Creative Commons License

TABLE A1. *Continued.* Bulk mineral volume abundances of the meteorites used in this study.

Sample	Group	Olivine	Low-Ca pyroxene	High-Ca pyroxene	Plagioclase	Phyllosilicates	Sulfide	FeNi-metal	Magnetite	Ferrihydrite	Carbonates	Gypsum	Other[a]	Reference
CHERVONY KUT	Eucrite		42.37	9.16	45.00									[8]
EET 87520	Eucrite		39.30	10.37	49.00									[8]
EET 900200	Eucrite		38.47	10.55	50.00									[8]
GRA 98098	Eucrite		42.78	7.41	41.00									[8]
GRO 95533	Eucrite		41.68	9.52	44.00									[8]
Ibitra	Eucrite		41.81	11.48	41.00									[8]
MAC 02522	Eucrite		17.47	39.53	41.00									[8]
MET 01081	Eucrite		45.83	7.17	40.00									[8]
Moore County	Eucrite		40.73	11.37	44.00									[8]
PCA 82501	Eucrite		39.42	9.38	44.00									[8]
PCA 91078	Eucrite		25.40	25.30	46.00									[8]
Serra de Mage	Eucrite		39.83	5.26	53.00									[8]
NWA 6013	Ol-rich diogenite	*27.64*	*62.79*	n.d.	*8.86*		n.d.						*0.72*	[6]
NWA 2968	Dunitic diogenite	*92.20*	*0.10*	n.d.	n.d.		*2.26*						*5.45*	[6]
Tatahouine	Diogenite	*0.11*	*97.98*	n.d.	n.d.		n.d.						*1.91*	[6]
Johnstown	Diogenite	3	85	3	3		3.00						1.5	[9]
ALH 85015	Diogenite	4.6	87.42	2.37	5.00									[8]
ALHA 77256	Diogenite	10.6	68.32	20.08	0.10									[8]
EET 83246	Diogenite	1.3	95.39	2.82	n.d.									[8]
GRA 98108	Diogenite	18.5	79.40	1.00	0.30									[8]
LAP02216	Diogenite	2	95.06	1.94	n.d.									[8]
LAP 03979	Diogenite	4.6	87.84	3.06	3.90									[8]
LEW 88008	Diogenite	1.6	91.24	4.37	2.20									[8]
LEW 88679	Diogenite	14.6	80.06	3.24	0.40									[8]
MET 01084	Diogenite	6.1	87.40	2.52	3.60									[8]
MIL 03368	Diogenite	2.2	92.73	2.87	n.d.									[8]
MIL 03443	Diogenite	91	5.23	0.46	n.d.									[8]
PCA 02008	Diogenite	3.7	91.75	2.35	1.30									[8]
QUE 99050	Diogenite	n.d.	96.04	1.76	n.d.									[8]

Note: Values in italic are converted from wt% using mean mineral densities. Where abundances were given in ranges, the mean value was used.

References: [1] King et al. (2015); [2]; Howard et al. (2015); [3]; Howard et al. (2010); [4]; Dunn et al. (2010); [5]; Fuhrman and Papike (1982); [6]; Cloutis et al. (2013); [7]; Kitts and Lodders (1998); Schwartz and McCallum (2001); [8]; Li and Milliken (2015); [9] Floran et al. (1977, 1981).

[a]Other: apatite, ilmenite, chromite.

19455100, 2023, 10, Downloaded from https://onlinelibrary.wiley.com/doi/10.1111/maps.14060 by Freie Universitaet Berlin, Wiley Online Library on [16/10/2023]. See the Terms and Conditions (https://onlinelibrary.wiley.com/terms-and-conditions) on Wiley Online Library for rules of use; OA articles are governed by the applicable Creative Commons License